Modeling Electromagnetic Fields

An Application in MRI

K. Koolstra

Technische Universiteit Delft

TU Delft Delft University of Technology

Challenge the future

MODELING ELECTROMAGNETIC FIELDS

AN APPLICATION IN MRI

by

K. Koolstra

Supervisor:	Dr. ir. M.B. van Gijzen,	TU Delft
	Dr. ir. R. Remis,	TU Delft
	MSc W. Brink,	LUMC
Thesis committee:	Dr. ir. M.B. van Gijzen,	TU Delft
	Dr. ir. R.F. Remis,	TU Delft
	Dr. J.L.A. Dubbeldam,	TU Delft
	Prof. dr. ir. C. Vuik,	TU Delft
	MSc W. Brink,	LUMC

TU Delft Delft University of Technology

Contents

1

INTRODUCTION

For decades scientists have been interested in modeling electromagnetic fields described by Maxwell's equations. These electromagnetic fields play a role in various applications.One of them is medical imaging, in which waves travel through a medium and are scattered by objects they meet. After measuring the scattered field, properties of the objects can be determined by solving a system of equations. Those problems are called inverse scattering problems. Sometimes the object is completely known and one is interested in how the electromagnetic waves propagate inside the object. The corresponding problems are called forward scattering problems.
In MRI (Magnetic Resonance Imaging) recent developments gave rise to modeling those forward problems. It was shown that placing dielectric pads between the human body and the receiver coil in an MRI scanner reduces artifacts in the constructed images as a result of reduced RF inhomogeneity [1]. Dielectric pads are pouches filled with a material that has a very high permittivity, which means that the PAD has the ability to affect the incoming electromagnetic wave considerably. In order to obtain the optimal image quality the geometry of the PAD is essential. Models that predict the electromagnetic fields are needed to determine the optimal parameters beforehand and in this way avoid trial and error.

There are different ways to solve Maxwell's equations. One group of methods chooses Maxwell's equations in partial differenital form as a starting point. The finite-difference time-domain (FDTD) and the finite element method (FEM) are examples of methods in this group. The other group rewrites Maxwell's equations into so-called volume integral equations, which are a form of integro-differential equations. The Method of Moments (MOM) is an example that deals with the volume integral equation. Even though methods in the latter group involve full matrices and are therefore computationally expensive, the Method of Moments is a popular method because the boundary conditions are automatically satisfied by choosing the basis functions wisely. The Method of Moments is based on discretising the volume integral equations on a chosen mesh and approximating the fields or related unknowns with the help of chosen basis and test functions.
In practical applications a short computation time is crucial, which is why one often chooses a structured grid consisting of voxels with the grid points lying at the centers. The equations of interest can be formulated in terms of the electric fields or in terms of the currents. These formulations form different starting points for a discretised system.

The main goal of this report is to make the reader familiar with the inaccuracy problem in one of the methods. To do so, different topics are discussed.
Chapter 2 starts with Maxwell's equations and its boundary conditions. These equations form the basis of each model. Also the volume integral form that is needed for the Method of Moments is derived here. Finally, different formulations of these volume integral equations are discussed, as it turns out that each of them leads to approximations with different accuracies.
In Chapter 3 the Method of Moments is explained in more detail. In order to provide the reader with a better understanding of the method, two examples are given in which the Method of Moments is demonstrated. The first one is our own derivation with a triangular mesh. The second one is the conventional method that is used to model the electromagnetic fields nowadays and it is also the one of which it is known that a problem occurs at permittivity interfaces.

In Chapter 4 there will be an elaboration on types of solution methods that can be used once a system of equations is obtained. Short computation time is the motivation.
In Chapter 5 a summary will be given of the existing approaches, including performance results and an overview of general advantages and drawbacks.
In Chapter 6 results from the second example are shown that demonstrate the inaccuracy at high permittivity interfaces. Also results from the first example are given to demonstrate some boundary problems.
Finally, in Chapter 7 the report will be concluded with ideas of approaches that could result in better accuracy.
Throughout the report constants will be presented upright, vectors will be presented upright in bold, matrices will be defined with capitals and scalar functions will be shown in italic script.

2

THE ELECTRIC AND MAGNETIC FIELDS IN MRI

The first step towards calculating the electric and magnetic fields is describing the fields mathematically. J.C. Maxwell did this a long time ago. In Section 2.1 this mathematical formulation is discussed. The boundary conditions that complement Maxwell's equations are derived in 2.2. In this study the focus lies on the volume integral equation approach, so in 2.3 the volume integral form is derived with its different formulations. The derivation of the first formulation can also be found in [2].

2.1. MAXWELL'S EQUATIONS

James Clerk Maxwell was a mathematician and physicist that formulated a set of equations describing how electric and magnetic fields propagate and interact. This set of equations forms the foundation of classical electrodynamics and is therefore very important in understanding the electromagnetic fields in MRI. Maxwell's equations are given by

$$-\nabla\times\mathbf{H}+\mathbf{J}+\frac{\partial\mathbf{D}}{\partial t} = -\mathbf{J}^{\text{ext}} \tag{2.1}$$

$$\nabla\times\mathbf{E}+\frac{\partial\mathbf{B}}{\partial t} = -\mathbf{K}^{\text{ext}}. \tag{2.2}$$

The variables $\mathbf{J}^{\text{ext}}$ and $\mathbf{K}^{\text{ext}}$ are the external sources and are therefore known. More specifically, the external magnetic source is always zero. Both sources start to act at $t=0$. The unknowns are related via the constitutive relations,

$$\mathbf{D} = \varepsilon\mathbf{E} \tag{2.3}$$

$$\mathbf{B} = \mu\mathbf{H} \tag{2.4}$$

$$\mathbf{J} = \sigma\mathbf{E}, \tag{2.5}$$

where σ is the conductivity of the material, ε is the permittivity and μ is the permeability. In this study only nonmagnetic media will be considered, which means that $\mu=\mu_0$ where μ_0 is the permeability of vacuum. The unknown fields are the electric field strength $\mathbf{E}$ and the magnetic field strength $\mathbf{H}$. Both fields vanish everywhere for $t<0$. $\mathbf{D}$ and $\mathbf{B}$ are the electric displacement field and the magnetic flux density respectively. To complete Maxwell's equations, the compatibility relations are derived by taking the divergence of (2.1) and (2.2). This yields

$$\nabla\cdot\mathbf{J}+\frac{\partial}{\partial t}\nabla\cdot\mathbf{D} = -\nabla\cdot\mathbf{J}^{\text{ext}} \tag{2.6}$$

$$\frac{\partial}{\partial t}\nabla\cdot\mathbf{B} = 0. \tag{2.7}$$

The total current is defined by $\mathbf{J}^{\text{tot}}=\mathbf{J}+\mathbf{J}^{\text{ext}}$ and $\nabla\cdot\mathbf{D}=\rho$. Then (2.6) becomes $\nabla\cdot\mathbf{J}^{\text{tot}}+\frac{\partial\rho}{\partial t}=0$, which means that there is conservation of charge. From (2.7) it follows that $\nabla\cdot\mathbf{B}$ is constant in time and because of the initial condition it follows that this constant is zero. Therefore,

$$\nabla \cdot \mathbf{D} = \rho \tag{2.8}$$
$$\nabla \cdot \mathbf{B} = 0. \tag{2.9}$$

Maxwell's equations describe that magnetic fields can be created by a change in electric field or by an electrical current. A changing magnetic field creates an electric field. The strength of the electric field is related to the distance away from the charge and the net magnetic flux is always zero.

2.2. BOUNDARY CONDITIONS

Maxwell's equations form a system of four equations. The equations are of first order, so from each of the equations a boundary condition can be derived. In order to find them, each of the four equations is integrated over a control volume or control area. In the derivation it is assumed that no external sources are present at the interfaces between different media.

TANGENTIAL COMPONENT OF **H**

Integration of (2.1) over a rectangular region that is given in Figure 2.1a and applying Stokes' theorem, gives

$$\begin{aligned} \int_A -\nabla \times \mathbf{H} + \mathbf{J} + \frac{\partial \mathbf{D}}{\partial t} \mathrm{d}A &= \mathbf{0} \Leftrightarrow \\ \int_{\partial A} -\mathbf{H} \times \mathbf{n} \mathrm{d}\Gamma + \int_A \mathbf{J} + \frac{\partial \mathbf{D}}{\partial t} \mathrm{d}A &= \mathbf{0}. \end{aligned}$$

As the height of the rectangle Δh drops to zero, the integral of the derivative term vanishes. In physical media the conduction is finite and therefore also $\mathbf{J}$. In that case the $\mathbf{J}$ term vanishes and

$$\begin{aligned} -\int_{\partial A_1} \mathbf{H}_1 \times \mathbf{n}_1 \mathrm{d}\Gamma_1 - \int_{\partial A_2} \mathbf{H}_2 \times \mathbf{n}_2 \mathrm{d}\Gamma_2 &= \mathbf{0} \Leftrightarrow \\ \mathbf{n} \times (\mathbf{H}_1 - \mathbf{H}_2) &= \mathbf{0}. \end{aligned}$$

This means that the tangential component of the magnetic field is continuous across the interface between different media.

TANGENTIAL COMPONENT OF **E**

Integration of (2.2) over a rectangular region that is given in Figure 2.1a and applying Stokes' theorem, gives

$$\begin{aligned} \int_A \nabla \times \mathbf{E} + \frac{\partial \mathbf{B}}{\partial t} \mathrm{d}A &= \mathbf{0} \Leftrightarrow \\ \int_{\partial A} \mathbf{E} \times \mathbf{n} \mathrm{d}\Gamma + \int_A \frac{\partial \mathbf{B}}{\partial t} \mathrm{d}A &= \mathbf{0}. \end{aligned}$$

As the height of the rectangle drops to zero, the integral of the derivative term vanishes. Therefore,

$$\begin{aligned} \int_{\partial A_1} \mathbf{E}_1 \times \mathbf{n}_1 \mathrm{d}\Gamma_1 + \int_{\partial A_2} \mathbf{E}_2 \times \mathbf{n}_2 \mathrm{d}\Gamma_2 &= \mathbf{0} \Leftrightarrow \\ \mathbf{n} \times (\mathbf{E}_1 - \mathbf{E}_2) &= \mathbf{0}. \end{aligned}$$

Also the tangential component of the electric field is continuous across the interface between different media.

NORMAL COMPONENT OF **D**

Integration of (2.6) over a cylinder that is shown in Figure 2.1b, gives

$$\begin{aligned} \int_V \nabla \cdot \left(\mathbf{J} + \frac{\partial \mathbf{D}}{\partial t} \right) \mathrm{d}V &= 0 \Leftrightarrow \\ \int_{\partial V} \left(\mathbf{J} + \frac{\partial \mathbf{D}}{\partial t} \right) \cdot \mathbf{n} \mathrm{d}\Gamma &= 0 \end{aligned}$$

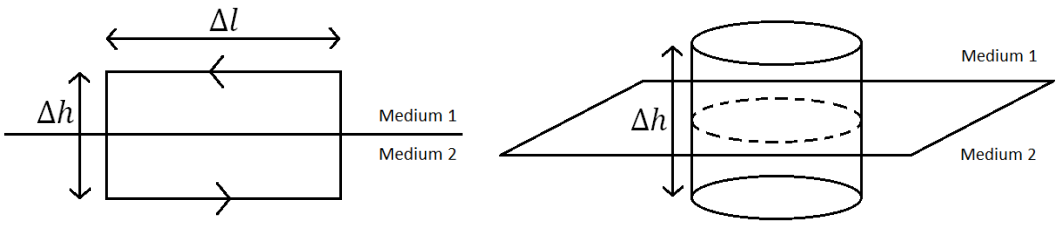

(a) Control area for deriving the tangential components of **H** and **E**.

(b) Control volume for deriving the normal components of **D** and **B**.

Figure 2.1

by the divergence theorem. Making the cylinder arbitrarily small in height, results in a vanishing integral over the curved surface $d\Gamma_3$. Since both sides of the interface may have different properties, distinction is made between $\mathbf{D}_1$ and $\mathbf{D}_2$. Therefore,

$$\begin{aligned}\int_{\partial V_1}\left(\mathbf{J}_1+\frac{\partial \mathbf{D}_1}{\partial t}\right)\cdot\mathbf{n}_1 d\Gamma_1+\int_{\partial V_2}\left(\mathbf{J}_2+\frac{\partial \mathbf{D}_2}{\partial t}\right)\cdot\mathbf{n}_2 d\Gamma_2 &= 0 \Leftrightarrow\\ \left(\left(\mathbf{J}_1+\frac{\partial \mathbf{D}_1}{\partial t}\right)-\left(\mathbf{J}_2+\frac{\partial \mathbf{D}_2}{\partial t}\right)\right)\cdot\mathbf{n} &= 0,\end{aligned}$$

which means that $\mathbf{J}+\frac{\partial \mathbf{D}}{\partial t}$ is continuous across the interface between different media.

NORMAL COMPONENT OF **B**

By integrating (2.9) over a cylinder that is shown in Figure 2.1b and applying the divergence theorem, a boundary condition can be derived for the magnetic flux density:

$$(\mathbf{B}_1-\mathbf{B}_2)\cdot\mathbf{n} = 0.$$

The normal component of the magnetic flux denisity is continuous across the interface between different media.
To summarise the findings, the boundary conditions corresponding to Maxwell's equations are given by

$$\begin{aligned}\mathbf{n}\times(\mathbf{E}_1-\mathbf{E}_2) &= \mathbf{0}\\ \left(\left(\mathbf{J}_1+\frac{\partial \mathbf{D}_1}{\partial t}\right)-\left(\mathbf{J}_2+\frac{\partial \mathbf{D}_2}{\partial t}\right)\right)\cdot\mathbf{n} &= 0\\ (\mathbf{B}_1-\mathbf{B}_2)\cdot\mathbf{n} &= 0\\ \mathbf{n}\times(\mathbf{H}_1-\mathbf{H}_2) &= \mathbf{0}.\end{aligned}$$

2.3. THE VOLUME INTEGRAL EQUATION

The solution of Maxwell's equations can be found by first rewriting Maxwell's equations into a different form: the Volume Integral Equation. This will be done for the general $3D$ case, from which also the $2D$ case can be derived. In the final form of this formulation both the unknowns **E** and **H** and their integrals are present, but the equations for **E** and **H** are now uncoupled. This means that they can be solved separately. To get there, consider first the Laplace transform of (2.1) and (2.2),

$$-\nabla\times\hat{\mathbf{H}}+\eta\hat{\mathbf{E}} = -\mathbf{J}^{\text{ext}} \tag{2.10}$$

$$\nabla\times\mathbf{E}+\zeta\hat{\mathbf{H}} = -\mathbf{K}^{\text{ext}}. \tag{2.11}$$

with the Laplace transform defined by

$$\hat{f}(\mathbf{x},s)=\mathscr{L}\{f(\mathbf{x},t)\}=\int_0^\infty f(\mathbf{x},t)e^{-st}dt$$

and $\eta=\sigma+s\varepsilon$, $\zeta=s\mu_0$. The compatibility relations then transform into

$$\nabla\cdot\eta\hat{\mathbf{E}} = -\nabla\cdot\hat{\mathbf{J}}^{\text{ext}} \tag{2.12}$$

$$\nabla\cdot\zeta\hat{\mathbf{H}} = -\nabla\cdot\hat{\mathbf{K}}^{\text{ext}}. \tag{2.13}$$

Now consider (2.10) and (2.11) for the medium vacuum. In that case, $\varepsilon = \varepsilon_0$ and $\sigma = 0$. This gives the system

$$-\nabla \times \hat{\mathbf{H}} + \eta_0 \hat{\mathbf{E}} = -\hat{\mathbf{J}}^{\text{ext}} \tag{2.14}$$
$$\nabla \times \hat{\mathbf{E}} + \zeta_0 \hat{\mathbf{H}} = -\hat{\mathbf{K}}^{\text{ext}}, \tag{2.15}$$

with $\eta_0 = s\varepsilon_0$ and $\zeta_0 = s\mu_0$.

Next a Fourier transform, defined by

$$\tilde{f}(\mathbf{k}, s) = \mathscr{F}\{f(\mathbf{x}, s)\} = \int_{\mathbf{x}\in\mathbb{R}^3} f(\mathbf{x}, s) e^{i\mathbf{k}\cdot\mathbf{x}} \mathrm{d}V,$$

transforms (2.14) and (2.15) into

$$i\mathbf{k} \times \tilde{\mathbf{H}} + \eta_0 \tilde{\mathbf{E}} = -\tilde{\mathbf{J}}^{\text{ext}} \tag{2.16}$$
$$-i\mathbf{k} \times \tilde{\mathbf{E}} + \zeta_0 \tilde{\mathbf{H}} = -\tilde{\mathbf{K}}^{\text{ext}}. \tag{2.17}$$

Note that in the last system both the time derivatives and the spatial derivatives are eliminated. This makes it much easier to find expressions for $\tilde{\mathbf{H}}$ and $\tilde{\mathbf{E}}$. (2.17) can be rewritten into

$$\tilde{\mathbf{H}} = \frac{1}{\zeta_0}\left(-\tilde{\mathbf{K}}^{\text{ext}} + \mathrm{i}\mathbf{k} \times \tilde{\mathbf{E}}\right) \tag{2.18}$$

after which $\tilde{\mathbf{H}}$ can be eliminated from (2.16). This yields

$$\left((\mathbf{k}^T\mathbf{k} + \gamma_0^2)\mathbf{I} - \mathbf{k}\mathbf{k}^T\right)\tilde{\mathbf{E}} = -\zeta_0 \tilde{\mathbf{J}}^{\text{ext}} + \mathrm{i}\mathbf{k} \times \tilde{\mathbf{K}}^{\text{ext}} \tag{2.19}$$

where $\zeta_0\eta_0 = \gamma_0^2$. It would be easy to solve (2.19) for $\tilde{\mathbf{E}}$ if the matrix in front of $\tilde{\mathbf{E}}$ were invertible. Unfortunately, in many cases this becomes a problem. Therefore a clever trick is used. The compatibility relations for Maxwell's equation in vacuum,

$$\eta_0 \nabla \cdot \hat{\mathbf{E}} = -\nabla \cdot \hat{\mathbf{J}}^{\text{ext}} \tag{2.20}$$
$$\zeta_0 \nabla \cdot \hat{\mathbf{H}} = -\nabla \cdot \hat{\mathbf{K}}^{\text{ext}}, \tag{2.21}$$

can be transformed into frequency domain,

$$\eta_0 \mathbf{k}^T \tilde{\mathbf{E}} = -\mathbf{k}^T \tilde{\mathbf{J}}^{\text{ext}}$$
$$\zeta_0 \mathbf{k}^T \tilde{\mathbf{H}} = -\mathbf{k}^T \tilde{\mathbf{K}}^{\text{ext}},$$

and these two equations turn out useful in rewriting the left hand side of (2.19) as

$$\left((\mathbf{k}^T\mathbf{k} + \gamma_0^2)\mathbf{I} - \mathbf{k}\mathbf{k}^T\right)\tilde{\mathbf{E}} = (\mathbf{k}^T\mathbf{k} + \gamma_0^2)\tilde{\mathbf{E}} + \frac{1}{\eta_0}\mathbf{k}\mathbf{k}^T\tilde{\mathbf{J}}^{\text{ext}}.$$

Now the new equation for $\tilde{\mathbf{E}}$ is given by

$$(\mathbf{k}^T\mathbf{k} + \gamma_0^2)\tilde{\mathbf{E}} + \frac{1}{\eta_0}\mathbf{k}\mathbf{k}^T\tilde{\mathbf{J}}^{\text{ext}} = -\zeta_0 \tilde{\mathbf{J}}^{\text{ext}} + \mathrm{i}\mathbf{k} \times \tilde{\mathbf{K}}^{\text{ext}}$$

from which $\tilde{\mathbf{E}}$ can be written as

$$\tilde{\mathbf{E}} = \frac{1}{\mathbf{k}^T\mathbf{k} + \gamma_0^2}\left(-(\zeta_0\mathbf{I} + \frac{1}{\eta_0}\mathbf{k}\mathbf{k}^T)\tilde{\mathbf{J}}^{\text{ext}} + \mathrm{i}\mathbf{k} \times \tilde{\mathbf{K}}^{\text{ext}}\right). \tag{2.22}$$

Substitution of (2.22) in (2.18) gives

$$\tilde{\mathbf{H}} = \frac{1}{\mathbf{k}^T\mathbf{k} + \gamma_0^2}\left(-\left(\eta_0\mathbf{I} + \frac{1}{\zeta_0}\mathbf{k}\mathbf{k}^T\right)\tilde{\mathbf{K}}^{\text{ext}} - \mathrm{i}\mathbf{k} \times \tilde{\mathbf{J}}^{\text{ext}}\right).$$

Now that expressions for $\tilde{\mathbf{E}}$ and $\tilde{\mathbf{H}}$ have been found, the next step is to transform the expressions back into $\mathbf{x}$ domain by applying the inverse Fourier transform. This is done by introducing the vector potentials $\tilde{\mathbf{A}}$ and $\tilde{\mathbf{F}}$:

$$\tilde{\mathbf{A}} = \tilde{g}\tilde{\mathbf{J}}^{\text{ext}}$$
$$\tilde{\mathbf{F}} = \tilde{g}\tilde{\mathbf{K}}^{\text{ext}},$$

where $\tilde{g} = \frac{1}{\mathbf{k}^T\mathbf{k}+\gamma_0^2}$ is the Green's function of the Helmholtz equation. In terms of these new variables the set of equations becomes

$$\begin{aligned}\tilde{\mathbf{E}} &= -\left(\zeta_0\mathbf{I}+\frac{1}{\eta_0}\mathbf{k}\mathbf{k}^T\right)\tilde{\mathbf{A}}+\mathrm{i}\mathbf{k}\times\tilde{\mathbf{F}}\\ \tilde{\mathbf{H}} &= -\left(\eta_0\mathbf{I}+\frac{1}{\zeta_0}\mathbf{k}\mathbf{k}^T\right)\tilde{\mathbf{F}}-\mathrm{i}\mathbf{k}\times\tilde{\mathbf{A}}\end{aligned}$$

and in Laplace domain

$$\hat{\mathbf{E}} = -\zeta_0\hat{\mathbf{A}}+\frac{1}{\eta_0}\nabla(\nabla\cdot\hat{\mathbf{A}})-\nabla\times\hat{\mathbf{F}} \tag{2.23}$$

$$\hat{\mathbf{H}} = -\eta_0\hat{\mathbf{F}}+\frac{1}{\zeta_0}\nabla(\nabla\cdot\hat{\mathbf{F}})+\nabla\times\hat{\mathbf{A}} \tag{2.24}$$

where

$$\begin{aligned}\hat{\mathbf{A}} &= \int_{\mathbf{x}'\in\mathbb{R}^3}\hat{g}(\mathbf{x}-\mathbf{x}',s)\hat{\mathbf{J}}^{\mathrm{ext}}(\mathbf{x}',s)\mathrm{d}V'\\ \hat{\mathbf{F}} &= \int_{\mathbf{x}'\in\mathbb{R}^3}\hat{g}(\mathbf{x}-\mathbf{x}',s)\hat{\mathbf{K}}^{\mathrm{ext}}(\mathbf{x}',s)\mathrm{d}V'\end{aligned}$$

by the convolution theorem.

The inverse Fourier transform of the Green's function for the $3D$ configuration is

$$\hat{g}(\mathbf{x},s) = \frac{e^{\mathrm{i}\mathrm{k}_\mathrm{b}|\mathbf{x}|}}{4\pi|\mathbf{x}|} \tag{2.25}$$

and for the $2D$ configuration the result is

$$\hat{g}(\mathbf{x},s) = -\frac{\mathrm{i}}{4}H_0^{(2)}(\mathrm{k}_\mathrm{b}|x|),$$

where

$$\gamma_0 = \mathrm{k}_\mathrm{b}\mathrm{i}.$$

The derivation for the $2D$ case can be found in Appendix A.

2.4. THE SCATTERING PROBLEM

So far it was assumed that the source is surrounded by vacuum. In many cases, including the MRI problem where the human body is a large object, this is not realistic. Charged particles in the object are influenced by the fields generated by the source. The charged particles start to oscillate in turn, which can be regarded as induced currents. In order to take these induced currents into account, Maxwell's equations are rewritten as

$$\begin{aligned}-\nabla\times\mathbf{H}+\varepsilon_0\frac{\partial\mathbf{E}}{\partial t} &= -\left(\mathbf{J}^{\mathrm{ind}}+\mathbf{J}^{\mathrm{ext}}\right)\\ \nabla\times\mathbf{E}+\mu_0\frac{\partial\mathbf{H}}{\partial t} &= -\left(\mathbf{K}^{\mathrm{ind}}+\mathbf{K}^{\mathrm{ext}}\right),\end{aligned}$$

where $\mathbf{J}^{\mathrm{ext}}$ and $\mathbf{K}^{\mathrm{ext}}$ are again the external sources and $\mathbf{J}^{\mathrm{ind}}$ and $\mathbf{K}^{\mathrm{ind}}$ are induced by the fields. With these new right hand sides of Maxwell's equations, it follows by substitution that the volume integral equations become

$$\begin{aligned}\hat{\mathbf{E}}(\mathbf{x},s) = &-\zeta_0\int_{\mathbf{x}'\in\mathbb{R}^3}\hat{g}(\mathbf{x}-\mathbf{x}',s)\left(\hat{\mathbf{J}}^{\mathrm{ext}}(\mathbf{x}',s)+\hat{\mathbf{J}}^{\mathrm{ind}}(\mathbf{x}',s)\right)\mathrm{d}V'+\frac{1}{\eta_0}\nabla\left(\nabla\cdot\int_{\mathbf{x}'\in\mathbb{R}^3}\hat{g}(\mathbf{x}-\mathbf{x}',s)\left(\hat{\mathbf{J}}^{\mathrm{ext}}(\mathbf{x}',s)+\hat{\mathbf{J}}^{\mathrm{ind}}(\mathbf{x}',s)\right)\mathrm{d}V'\right)\\ &-\nabla\times\int_{\mathbf{x}'\in\mathbb{R}^3}\hat{g}(\mathbf{x}-\mathbf{x}',s)\left(\hat{\mathbf{K}}^{\mathrm{ext}}(\mathbf{x}',s)+\hat{\mathbf{K}}^{\mathrm{ind}}(\mathbf{x}',s)\right)\mathrm{d}V'\end{aligned} \tag{2.26}$$

$$\begin{aligned}\hat{\mathbf{H}}(\mathbf{x},s) = &-\eta_0\int_{\mathbf{x}'\in\mathbb{R}^3}\hat{g}(\mathbf{x}-\mathbf{x}',s)\left(\hat{\mathbf{K}}^{\mathrm{ext}}(\mathbf{x}',s)+\hat{\mathbf{K}}^{\mathrm{ind}}(\mathbf{x}',s)\right)\mathrm{d}V'+\frac{1}{\zeta_0}\nabla\left(\nabla\cdot\int_{\mathbf{x}'\in\mathbb{R}^3}\hat{g}(\mathbf{x}-\mathbf{x}',s)\left(\hat{\mathbf{K}}^{\mathrm{ext}}(\mathbf{x}',s)+\hat{\mathbf{K}}^{\mathrm{ind}}(\mathbf{x}',s)\right)\mathrm{d}V'\right)\\ &+\nabla\times\int_{\mathbf{x}'\in\mathbb{R}^3}\hat{g}(\mathbf{x}-\mathbf{x}',s)\left(\hat{\mathbf{J}}^{\mathrm{ext}}(\mathbf{x}',s)+\hat{\mathbf{J}}^{\mathrm{ind}}(\mathbf{x}',s)\right)(\mathbf{x}',s)\mathrm{d}V'.\end{aligned} \tag{2.27}$$

There is a relation between the total field with object present and the electromagnetic fields in vacuum where no object is present. The difference between those two fields is the field radiated by the induced currents, called the scattered field. This can be written as

$$\mathbf{E}^{\text{sc}} = \mathbf{E} - \mathbf{E}^{\text{inc}} \tag{2.28}$$
$$\mathbf{H}^{\text{sc}} = \mathbf{H} - \mathbf{H}^{\text{inc}}, \tag{2.29}$$

where $\mathbf{E}^{\text{inc}}$ and $\mathbf{H}^{\text{inc}}$ are the fields in vacuum (inc is short for incident) and are given by

$$\begin{aligned}\hat{\mathbf{E}}^{\text{inc}}(\mathbf{x},s) = &-\zeta_0 \int_{\mathbf{x}'\in\mathbb{R}^3} \hat{g}(\mathbf{x}-\mathbf{x}',s)\hat{\mathbf{J}}^{\text{ext}}(\mathbf{x}',s)\mathrm{d}V' + \frac{1}{\eta_0}\nabla\left(\nabla\cdot\int_{\mathbf{x}'\in\mathbb{R}^3} \hat{g}(\mathbf{x}-\mathbf{x}',s)\hat{\mathbf{J}}^{\text{ext}}(\mathbf{x}',s)\mathrm{d}V'\right)\\ &-\nabla\times\int_{\mathbf{x}'\in\mathbb{R}^3} \hat{g}(\mathbf{x}-\mathbf{x}',s)\hat{\mathbf{K}}^{\text{ext}}(\mathbf{x}',s)\mathrm{d}V' \end{aligned}\tag{2.30}$$

$$\begin{aligned}\hat{\mathbf{H}}^{\text{inc}}(\mathbf{x},s) = &-\eta_0 \int_{\mathbf{x}'\in\mathbb{R}^3} \hat{g}(\mathbf{x}-\mathbf{x}',s)\hat{\mathbf{K}}^{\text{ext}}(\mathbf{x}',s)\mathrm{d}V' + \frac{1}{\zeta_0}\nabla\left(\nabla\cdot\int_{\mathbf{x}'\in\mathbb{R}^3} \hat{g}(\mathbf{x}-\mathbf{x}',s)\hat{\mathbf{K}}^{\text{ext}}(\mathbf{x}',s)\mathrm{d}V'\right)\\ &+\nabla\times\int_{\mathbf{x}'\in\mathbb{R}^3} \hat{g}(\mathbf{x}-\mathbf{x}',s)\hat{\mathbf{J}}^{\text{ext}}(\mathbf{x}',s)\mathrm{d}V' \end{aligned}\tag{2.31}$$

according to Maxwell's equations. It is important to note that the incident fields are known, because they are determined by the external sources in vacuum and a closed-form solution is available. Substracting (2.30) and (2.31) from (2.26) and (2.27) give expressions for the scattered fields and these can be substituted in (2.28) and (2.29) to find

$$\begin{aligned}\hat{\mathbf{E}}^{\text{inc}}(\mathbf{x},s) = &\hat{\mathbf{E}}(\mathbf{x},s) + \zeta_0 \int_{\mathbf{x}'\in\mathbb{R}^3} \hat{g}(\mathbf{x}-\mathbf{x}',s)\hat{\mathbf{J}}^{\text{ind}}(\mathbf{x}',s)\mathrm{d}V' - \frac{1}{\eta_0}\nabla\left(\nabla\cdot\int_{\mathbf{x}'\in\mathbb{R}^3} \hat{g}(\mathbf{x}-\mathbf{x}',s)\hat{\mathbf{J}}^{\text{ind}}(\mathbf{x}',s)\mathrm{d}V'\right)\\ &+\nabla\times\int_{\mathbf{x}'\in\mathbb{R}^3} \hat{g}(\mathbf{x}-\mathbf{x}',s)\hat{\mathbf{K}}^{\text{ind}}(\mathbf{x}',s)\mathrm{d}V' \end{aligned}\tag{2.32}$$

$$\begin{aligned}\hat{\mathbf{H}}^{\text{inc}}(\mathbf{x},s) = &\hat{\mathbf{H}}(\mathbf{x},s) + \eta_0 \int_{\mathbf{x}'\in\mathbb{R}^3} \hat{g}(\mathbf{x}-\mathbf{x}',s)\hat{\mathbf{K}}^{\text{ind}}(\mathbf{x}',s)\mathrm{d}V' - \frac{1}{\xi_0}\nabla\left(\nabla\cdot\int_{\mathbf{x}'\in\mathbb{R}^3} \hat{g}(\mathbf{x}-\mathbf{x}',s)\hat{\mathbf{K}}^{\text{ind}}(\mathbf{x}',s)\mathrm{d}V'\right)\\ &-\nabla\times\int_{\mathbf{x}'\in\mathbb{R}^3} \hat{g}(\mathbf{x}-\mathbf{x}',s)\hat{\mathbf{J}}^{\text{ind}}(\mathbf{x}',s)\mathrm{d}V'. \end{aligned}\tag{2.33}$$

Together (2.32) and (2.33) still contain four unknowns, which makes it impossible to solve for the fields $\hat{\mathbf{E}}$ and $\hat{\mathbf{H}}$. In order to eliminate the unknowns $\hat{\mathbf{K}}^{\text{ind}}$ and $\hat{\mathbf{J}}^{\text{ind}}$ the following relations are introduced:

$$\mathbf{J}^{\text{ind}} = \mathbf{J} + \frac{\partial}{\partial t}(\mathbf{D} - \varepsilon_0\mathbf{E}) \tag{2.34}$$
$$\mathbf{K}^{\text{ind}} = \frac{\partial}{\partial t}(\mathbf{B} - \mu_0\mathbf{H}), \tag{2.35}$$

where $\mathbf{J}$ is the electric current density produced by freely moving charged particles. Furthermore, the constitutive relations in Laplace domain,

$$\hat{\mathbf{D}}(\mathbf{x},s) = \varepsilon(\mathbf{x},s)\hat{\mathbf{E}}(\mathbf{x},s) \tag{2.36}$$
$$\hat{\mathbf{B}}(\mathbf{x},s) = \mu(\mathbf{x},s)\hat{\mathbf{H}}(\mathbf{x},s) \tag{2.37}$$
$$\hat{\mathbf{J}}(\mathbf{x},s) = \sigma(\mathbf{x},s)\hat{\mathbf{E}}(\mathbf{x},s), \tag{2.38}$$

turn out useful in finding expressions for $\hat{\mathbf{J}}^{\text{ind}}$ and $\hat{\mathbf{K}}^{\text{ind}}$ that depend on the unknowns $\hat{\mathbf{E}}$ and $\hat{\mathbf{H}}$ only. The result is obtained via transforming (2.34) and (2.35) into Laplace domain and substituting (2.36) - (2.38). The result is given by

$$\begin{aligned}\hat{\mathbf{J}}^{\text{ind}}(\mathbf{x},s) = &\left(\sigma(\mathbf{x},s) + s(\varepsilon(\mathbf{x},s) - \varepsilon_0(\mathbf{x},s))\right)\hat{\mathbf{E}}(\mathbf{x},s) &&= \left(\eta(\mathbf{x},s) - \eta_0(\mathbf{x},s)\right)\hat{\mathbf{E}}(\mathbf{x},s)\\ \hat{\mathbf{K}}^{\text{ind}}(\mathbf{x},s) = &\quad s\left(\mu(\mathbf{x},s) - \mu_0(\mathbf{x},s)\right)\hat{\mathbf{H}}(\mathbf{x},s) &&= \left(\xi(\mathbf{x},s) - \zeta_0(\mathbf{x},s)\right)\hat{\mathbf{H}}(\mathbf{x},s).\end{aligned}$$

Finally,

$$\hat{\mathbf{E}}^{\text{inc}}(\mathbf{x},s) = \hat{\mathbf{E}}(\mathbf{x},s)+\zeta_0(s)\eta_0(s)\int_{\mathbf{x}'\in\mathbb{R}^3}\hat{g}(\mathbf{x}-\mathbf{x}',s)\chi_{\text{e}}(\mathbf{x}',s)\hat{\mathbf{E}}(\mathbf{x}',s)\mathrm{d}V' - \nabla\left(\nabla\cdot\int_{\mathbf{x}'\in\mathbb{R}^3}\hat{g}(\mathbf{x}-\mathbf{x}',s)\chi_{\text{e}}(\mathbf{x}',s)\hat{\mathbf{E}}(\mathbf{x}',s)\mathrm{d}V'\right) + \xi_0(s)\nabla\times\int_{\mathbf{x}'\in\mathbb{R}^3}\hat{g}(\mathbf{x}-\mathbf{x}',s)\chi_{\text{m}}(\mathbf{x}',s)\hat{\mathbf{H}}(\mathbf{x}',s)\mathrm{d}V' \tag{2.39}$$

$$\hat{\mathbf{H}}^{\text{inc}}(\mathbf{x},s) = \hat{\mathbf{H}}(\mathbf{x},s)+\eta_0(s)\zeta_0(s)\int_{\mathbf{x}'\in\mathbb{R}^3}\hat{g}(\mathbf{x}-\mathbf{x}',s)\chi_{\text{m}}(\mathbf{x}',s)\hat{\mathbf{H}}(\mathbf{x}',s)\mathrm{d}V' - \nabla\left(\nabla\cdot\int_{\mathbf{x}'\in\mathbb{R}^3}\hat{g}(\mathbf{x}-\mathbf{x}',s)\chi_{\text{m}}(\mathbf{x}',s)\hat{\mathbf{H}}(\mathbf{x}',s)\mathrm{d}V'\right) - \eta_0(s)\nabla\times\int_{\mathbf{x}'\in\mathbb{R}^3}\hat{g}(\mathbf{x}-\mathbf{x}',s)\chi_{e}(\mathbf{x}',s)\hat{\mathbf{E}}(\mathbf{x}',s)\mathrm{d}V' \tag{2.40}$$

where the contrast functions are defined by

$$\chi_{\text{e}}(\mathbf{x},s) = \frac{\eta(\mathbf{x},s)}{\eta_0(s)}-1$$
$$\chi_{\text{m}}(\mathbf{x},s) = \frac{\xi(\mathbf{x},s)}{\zeta_0}-1.$$

In the human body the magnetic contrast χ_m is zero, so in this research (2.39) and (2.40) simplify to

$$\hat{\mathbf{E}}^{\text{inc}}(\mathbf{x},s) = \hat{\mathbf{E}}(\mathbf{x},s)+\zeta_0(s)\eta_0(s)\int_{\mathbf{x}'\in\mathbb{R}^3}\hat{g}(\mathbf{x}-\mathbf{x}',s)\chi_{e}(\mathbf{x}',s)\hat{\mathbf{E}}(\mathbf{x}',s)\mathrm{d}V' - \nabla\left(\nabla\cdot\int_{\mathbf{x}'\in\mathbb{R}^3}\hat{g}(\mathbf{x}-\mathbf{x}',s)\chi_{\text{e}}(\mathbf{x}',s)\hat{\mathbf{E}}(\mathbf{x}',s)\mathrm{d}V'\right) \tag{2.41}$$

$$\hat{\mathbf{H}}^{\text{inc}}(\mathbf{x},s) = \hat{\mathbf{H}}(\mathbf{x},s)-\eta_0(s)\nabla\times\int_{\mathbf{x}'\in\mathbb{R}^3}\hat{g}(\mathbf{x}-\mathbf{x}',s)\chi_{\text{e}}(\mathbf{x}',s)\hat{\mathbf{E}}(\mathbf{x}',s)\mathrm{d}V' \tag{2.42}$$

and these last two equations form the basis of the volume integral approach.

2.4.1. DIFFERENT FORMULATIONS OF THE SCATTERING PROBLEM

In the last paragraph (2.41) and (2.42) define two volume integral equations derived from Maxwell's equations. However, (2.36) - (2.38) allow for altering the derived volume integral equations. In this research the volume integral equation for the magnetic field will not be considered, because once the electric field is known, also the magnetic field can be found by substitution. Four different formulations will be discussed here. In rewriting the formulations, the relation $\hat{\mathbf{D}}_{\text{c}} = \varepsilon_c\hat{\mathbf{E}} = \frac{\eta}{s}\hat{\mathbf{E}} = (\frac{\sigma}{s}+\varepsilon)\hat{\mathbf{E}}$ is often introduced.

EVIE

The first one has already been derived in the beginning of this section, namely the EVIE (Electric Volume Integral Equation) formulation:

$$\hat{\mathbf{E}}^{\text{inc}}(\mathbf{x},s) = \hat{\mathbf{E}}(\mathbf{x},s) - \left(\mathrm{k}_{\text{b}}^2+\nabla\nabla\cdot\right)\mathbf{S}(\chi_{\text{e}}\hat{\mathbf{E}}) \tag{2.43}$$

where

$$\mathbf{S}(\mathbf{J}) = \int_{\Omega}\hat{g}(\mathbf{x}-\mathbf{x}',s)\mathbf{J}(\mathbf{x}',s)\mathrm{d}V'$$

and $\mathrm{k}_{\text{b}}^2 = -\zeta_0\eta_0$. The other formulations are based on the EVIE formulation.

DVIE

Substitution of the relation $\hat{\mathbf{D}}_c = \varepsilon_c\hat{\mathbf{E}}$ in (2.43) gives the DVIE formulation:

$$\hat{\mathbf{E}}^{\text{inc}}(\mathbf{x},s) = \frac{1}{\varepsilon_c}\hat{\mathbf{D}}_{\text{c}}(\mathbf{x},s) - (\mathrm{k}_{\text{b}}^2+\nabla\nabla\cdot)\mathbf{S}(\frac{\chi_{\text{e}}}{\varepsilon_c}\hat{\mathbf{D}}_{\text{c}}). \tag{2.44}$$

JVIE

Substitution of the relation $\hat{\mathbf{J}} = \eta_0\chi_{\text{e}}\hat{\mathbf{E}} = \sigma\hat{\mathbf{E}} + s\hat{\mathbf{E}}(\varepsilon-\varepsilon_0)$ in (2.43) gives the JVIE formulation:

$$\hat{\mathbf{E}}^{\text{inc}}(\mathbf{x},s) = \frac{1}{\eta_0\chi_{\text{e}}(\mathbf{x},s)}\hat{\mathbf{J}}(\mathbf{x},s) - \frac{1}{\eta_0}\left(\mathrm{k}_{\text{b}}^2+\nabla\nabla\cdot\right)\mathbf{S}(\hat{\mathbf{J}}). \tag{2.45}$$

In the last formulation a problem would occur if the contrast is zero. Therefore the JVIE is usually formulated as

$$\eta_0 \chi_e(\mathbf{x}, s)\hat{\mathbf{E}}^{\text{inc}}(\mathbf{x}, s) = \hat{\mathbf{J}}(\mathbf{x}, s) - \chi_e(\mathbf{x}, s)\left(k_b^2 + \nabla\nabla\cdot\right)\mathbf{S}(\hat{\mathbf{J}}). \tag{2.46}$$

For the above three formulations it has been shown in [3] that they are equivalent, that a unique solution exists and that the problems are well-posed in their corresponding function spaces. The corresponding function spaces will be discussed at the end of this subsection.

With the help of the identity $\nabla \times \nabla \times \mathbf{S}(\mathbf{F}) = \nabla\nabla \cdot \mathbf{F} - \nabla^2\mathbf{F}$ and the knowledge that the operator $\mathbf{S}$ satisfies the inhomogeneous Helmholtz equation $\nabla^2\mathbf{S}(\mathbf{F}) + k_b^2\mathbf{S}(\mathbf{F}) = -\mathbf{F}$, the expression $(k_b^2 + \nabla\nabla\cdot)\mathbf{S}(\mathbf{F})$ can be written as

$$(k_b^2 + \nabla\nabla\cdot)\mathbf{S}(\mathbf{F}) = \nabla \times \nabla \times \mathbf{S}(\mathbf{F}) - \mathbf{F}. \tag{2.47}$$

Now each of the three discussed formulations can be written in another form.

EVIE IN CURL FORM

Substitution of (2.47) in (2.43) gives

$$\hat{\mathbf{E}}^{\text{inc}}(\mathbf{x}, s) = (1 + \chi_e(\mathbf{x}, s))\hat{\mathbf{E}}(\mathbf{x}, s) - \nabla \times \nabla \times \mathbf{S}(\chi_e\hat{\mathbf{E}}). \tag{2.48}$$

DVIE IN CURL FORM

Substitution of (2.47) in (2.44) gives

$$\hat{\mathbf{E}}^{\text{inc}}(\mathbf{x}, s) = \frac{1}{\varepsilon_c}(1 + \chi_e(\mathbf{x}, s))\mathbf{D}_c(\mathbf{x}, s) - \nabla \times \nabla \times \mathbf{S}(\frac{\chi_e}{\varepsilon_c}\hat{\mathbf{D}}_c). \tag{2.49}$$

JVIE IN CURL FORM

Substitution of (2.47) in (2.45) gives

$$\eta_0 \chi_e(\mathbf{x}, s)\hat{\mathbf{E}}^{\text{inc}}(\mathbf{x}, s) = (1 + \chi_e(\mathbf{x}, s))\mathbf{J}(\mathbf{x}, s) - \chi_e(\mathbf{x}, s)\nabla \times \nabla \times \mathbf{S}(\hat{\mathbf{J}}) \tag{2.50}$$

or rewritten as in [4]:

$$\frac{\eta_0 \chi_e(\mathbf{x}, s)}{(1 + \chi_e(\mathbf{x}, s))}\hat{\mathbf{E}}^{\text{inc}}(\mathbf{x}, s) = \hat{\mathbf{J}}(\mathbf{x}, s) - \frac{\chi_e(\mathbf{x}, s)}{(1 + \chi_e(\mathbf{x}, s))}\nabla \times \nabla \times \mathbf{S}(\hat{\mathbf{J}}). \tag{2.51}$$

Although the first three formulations are very similar and the last three formulations as well, there is a difference between them that becomes clear when studying the domain and the range of the operators corresponding with the equations (2.43)-(2.50). The domains of the operators follow from Maxwell's equations, since $\mathbf{E}$ satisfies a curl equation and $\mathbf{D}$ a divergence equation. $\mathbf{J}$ is expected to live in $[L^2(\mathbb{R}^3)]^3$ because of the radiation conditions, [3].
The ranges of the operators in the first three formulations are derived in [3]. The ranges of the operators in the second three formulations are given in [4]. Summarised, the different formulations have the following mapping properties:

$$\begin{array}{llll} \text{EVIE:} & H(\text{curl}, \mathbb{R}^3) \mapsto H(\text{curl}, \mathbb{R}^3) & \text{EVIE curl:} & H(\text{curl}, \mathbb{R}^3) \mapsto H(\text{div}, \mathbb{R}^3) \\ \text{DVIE:} & H(\text{div}, \mathbb{R}^3) \mapsto H(\text{curl}, \mathbb{R}^3) & \text{DVIE curl:} & H(\text{div}, \mathbb{R}^3) \mapsto H(\text{curl}, \mathbb{R}^3) \\ \text{JVIE:} & [L^2(\mathbb{R}^3)]^3 \mapsto [L^2(\mathbb{R}^3)]^3 & \text{JVIE curl:} & [L^2(\mathbb{R}^3)]^3 \mapsto [L^2(\mathbb{R}^3)]^3. \end{array}$$

where

$$H(\text{curl}, \mathbb{R}^3) = \left\{f | f \in L^2(\mathbb{R}^3) \wedge \nabla \times f \in L^2(\mathbb{R}^3)\right\}$$

and

$$H(\text{div}, \mathbb{R}^3) = \left\{f | f \in L^2(\mathbb{R}^3) \wedge \nabla \cdot f \in L^2(\mathbb{R}^3)\right\}.$$

In the remainder of this report (2.43) will be used to demonstrate the principles of modeling electromagnetics.

3

THE METHOD OF MOMENTS

The Method of Moments is the most popular method to solve the volume integral equation. The reason for this is that Sommerfeld's radiation condition is automatically satisfied, so one does not have to deal with absorbing boundary conditions like in FEM or FDTD to obtain a unique solution. The steps in this procedure are similar to the ones in the Finite Element Method, but the resulting system matrix is full instead of banded. The first step is deriving the weak form of the volume integral equation. Once the weak form is obtained, the discretisation procedure begins by approximating the unknown by a sum of basisfunctions multiplied with unknown coefficients. These coefficients are the ones that need to be solved from the final system. To be able to do so, basis functions are chosen in such a way that they span the solution space and that the coefficients are easy to obtain. Two choices of test functions are commonly used. One results in Galerkin's Method and the other one in the Point Callocation Method. Both of these methods will be described in this chapter. Finally, two examples in which Galerkin's Method is used are given.

3.1. WEAK FORM

From this point on, the method will be explained for the $2D$ case. In the $2D$ configuration

$$\hat{\mathbf{E}}^{\text{inc}} = \hat{\mathbf{E}} + (\xi_0\eta_0 - \nabla\nabla\cdot)\,\mathbf{S}(\chi_e\hat{\mathbf{E}})$$

is a system of two coupled equations, where the electric field $\mathbf{E}$ is a vectorial unknown. Therefore two weak forms are derived. By doing this, both the x-component and the y-component of the electric field can be expanded with (possibly) different basis functions and different coefficients in the next step. In order to derive these two weak forms, the system is written in seperate equations for the two components:

$$\hat{E}_x^{\text{inc}} = \hat{E}_x + \xi_0\eta_0 S(\chi_e\hat{E}_x) - \frac{\partial}{\partial x}\left(\frac{\partial}{\partial x}S(\chi_e\hat{E}_x) + \frac{\partial}{\partial y}S(\chi_e\hat{E}_y)\right) \tag{3.1}$$

$$\hat{E}_y^{\text{inc}} = \hat{E}_y + \xi_0\eta_0 S(\chi_e\hat{E}_y) - \frac{\partial}{\partial y}\left(\frac{\partial}{\partial x}S(\chi_e\hat{E}_x) + \frac{\partial}{\partial y}S(\chi_e\hat{E}_y)\right) \tag{3.2}$$

where

$$S(J_\alpha) = \int_\Omega \hat{g}(\mathbf{x}-\mathbf{x}', s)J_\alpha(\mathbf{x}', s)\mathrm{d}V'.$$

Multiplication of (3.1) and (3.2) by test functions η_x and η_y respectively and integrating over the domain of interest Ω, gives

$$\int_\Omega \hat{E}_x^{\text{inc}}\eta_x\mathrm{d}\Omega = \int_\Omega \hat{E}_x\eta_x\mathrm{d}\Omega + \xi_0\eta_0\int_\Omega S(\chi_e\hat{E}_x)\eta_x\mathrm{d}\Omega - \int_\Omega \frac{\partial}{\partial x}\left(\nabla\cdot\mathbf{S}(\chi_e\hat{\mathbf{E}})\right)\eta_x\mathrm{d}\Omega \tag{3.3}$$

$$\int_\Omega \hat{E}_y^{\text{inc}}\eta_y\mathrm{d}\Omega = \int_\Omega \hat{E}_y\eta_y\mathrm{d}\Omega + \xi_0\eta_0\int_\Omega S(\chi_e\hat{E}_y)\eta_y\mathrm{d}\Omega - \int_\Omega \frac{\partial}{\partial y}\left(\nabla\cdot\mathbf{S}(\chi_e\hat{\mathbf{E}})\right)\eta_y\mathrm{d}\Omega. \tag{3.4}$$

Partial integrating and using Green's theorem, transforms the weak formulations (3.3) and (3.4) into

$$\int_\Omega \hat{E}_x^{\text{inc}}\eta_x \mathrm{d}\Omega = \int_\Omega \hat{E}_x\eta_x \mathrm{d}\Omega + \xi_0\eta_0\int_\Omega S(\chi_e\hat{E}_x)\eta_x \mathrm{d}\Omega + \int_\Omega \nabla\cdot\mathbf{S}(\chi_e\hat{\mathbf{E}})\frac{\partial}{\partial x}\eta_x \mathrm{d}\Omega - \int_{\partial\Omega}\nabla\cdot\mathbf{S}(\chi_e\hat{\mathbf{E}})\eta_x \mathrm{d}\Gamma \quad (3.5)$$

$$\int_\Omega \hat{E}_y^{\text{inc}}\eta_y \mathrm{d}\Omega = \int_\Omega \hat{E}_y\eta_y \mathrm{d}\Omega + \xi_0\eta_0\int_\Omega S(\chi_e\hat{E}_y)\eta_y \mathrm{d}\Omega + \int_\Omega \nabla\cdot\mathbf{S}(\chi_e\hat{\mathbf{E}})\frac{\partial}{\partial y}\eta_y \mathrm{d}\Omega - \int_{\partial\Omega}\nabla\cdot\mathbf{S}(\chi_e\hat{\mathbf{E}})\eta_y \mathrm{d}\Gamma. \quad (3.6)$$

Both weak formulations can be used to discretise the system. The advantage of the second weak form is that one spatial derivative now acts on the test function and is very easy to calculate. Moreover, the first derivative of the green's function contains a singularity that is weaker than the singularity of the second derivative of the green's function. The boundary terms in the second weak form are not implemented in reality, because on the boundary the contrast can always be chosen zero.

3.2. DISCRETISATION

Now that the weak forms are known, the volume integral equation can be transformed into a discretised system of equations. This can be done in several ways. The first possibility is approximating the unknowns $\hat{E}_x$ and $\hat{E}_y$ by series $\hat{E}_x^{\text{n}}(\mathbf{x}) = \sum_{j=1}^{\text{n}} e_{j,x}\phi_{j,x}(\mathbf{x})$ and $\hat{E}_y^{\text{n}}(\mathbf{x}) = \sum_{j=1}^{\text{n}} e_{j,y}\phi_{j,y}(\mathbf{x})$ that converge to $\hat{E}_x$ and $\hat{E}_y$ as $\text{n}\to\infty$. The second possibility is to expand not only the unknown electric field, but also the vector potential $\mathbf{S}(\chi_e\hat{\mathbf{E}})$ that operates on the unknown electric field. Additional substitutions $S_x^{\text{n}}(\mathbf{x}) = S^{\text{n}}(\chi_{\text{e}}\hat{E}_x)(\mathbf{x}) = \sum_{j=1}^{\text{n}} s_{j,x}\phi_{j,x}(\mathbf{x})$ and $S_y^{\text{n}}(\mathbf{x}) = S^{\text{n}}(\chi_{\text{e}}\hat{E}_y)(\mathbf{x}) = \sum_{j=1}^{\text{n}} s_{j,y}\phi_{j,y}(\mathbf{x})$ are carried out in this case. Also the incident field can be expanded.

3.2.1. EXPANDING THE ELECTRIC FIELD

Substitution of $\hat{E}_x^{\text{n}}$ and $\hat{E}_y^{\text{n}}$ in (3.3) and (3.4) respectively results in

$$\begin{aligned}
\int_\Omega \hat{E}_x^{\text{inc}}\eta_{i,x}\mathrm{d}\Omega &= \sum_{j=1}^{\text{n}} e_{j,x}\left\{\int_\Omega \phi_{j,x}\eta_{i,x}\mathrm{d}\Omega + \xi_0\eta_0\int_\Omega S(\chi_{\text{e}}\phi_{j,x})\eta_{i,x}\mathrm{d}\Omega - \int_\Omega \eta_{i,x}\frac{\partial}{\partial x}\frac{\partial}{\partial x}S(\chi_{\text{e}}\phi_{j,x})\mathrm{d}\Omega\right\} \\
&\quad - \sum_{j=1}^{\text{n}} e_{j,y}\left\{\int_\Omega \eta_{i,x}\frac{\partial}{\partial x}\frac{\partial}{\partial y}S(\chi_{\text{e}}\phi_{j,y})\mathrm{d}\Omega\right\} \qquad i = 1,..,\text{n} \\
\int_\Omega \hat{E}_y^{\text{inc}}\eta_{i,y}\mathrm{d}\Omega &= \sum_{j=1}^{\text{n}} e_{j,y}\left\{\int_\Omega \phi_{j,y}\eta_{i,y}\mathrm{d}\Omega + \xi_0\eta_0\int_\Omega S(\chi_{\text{e}}\phi_{j,y})\eta_{i,y}\mathrm{d}\Omega - \int_\Omega \eta_{i,y}\frac{\partial}{\partial y}\frac{\partial}{\partial y}S(\chi_e\phi_{j,y})\mathrm{d}\Omega\right\} \\
&\quad - \sum_{j=1}^{\text{n}} e_{j,x}\left\{\int_\Omega \eta_{i,y}\frac{\partial}{\partial y}\frac{\partial}{\partial x}S(\chi_{\text{e}}\phi_{j,x})\mathrm{d}\Omega\right\} \qquad i = 1,..,\text{n}.
\end{aligned}$$

Also, substitution of $\hat{E}_x^{\text{n}}$ and $\hat{E}_y^{\text{n}}$ in (3.5) and (3.6) respectively results in

$$\begin{aligned}
\int_\Omega \hat{E}_x^{\text{inc}}\eta_{i,x}\mathrm{d}\Omega &= \sum_{j=1}^{\text{n}} e_{j,x}\left\{\int_\Omega \phi_{j,x}\eta_{i,x}\mathrm{d}\Omega + \xi_0\eta_0\int_\Omega S(\chi_{\text{e}}\phi_{j,x})\eta_{i,x}\mathrm{d}\Omega\right. \\
&\quad \left. + \int_\Omega \frac{\partial}{\partial x}S(\chi_{\text{e}}\phi_{j,x})\frac{\partial}{\partial x}\eta_{i,x}d\Omega - \int_{\partial\Omega}\eta_{i,x}\frac{\partial}{\partial x}S(\chi_{\text{e}}\phi_{j,x})\mathrm{d}\Gamma\right\} \\
&\quad + \sum_{j=1}^{\text{n}} e_{j,y}\left\{\int_\Omega \frac{\partial}{\partial y}S(\chi_{\text{e}}\phi_{j,y})\frac{\partial}{\partial x}\eta_{i,x}\mathrm{d}\Omega - \int_{\partial\Omega}\eta_{i,x}\frac{\partial}{\partial y}S(\chi_{\text{e}}\phi_{j,y})\mathrm{d}\Gamma\right\} \qquad i = 1,..,\text{n} \\
\int_\Omega \hat{E}_y^{\text{inc}}\eta_{i,y}\mathrm{d}\Omega &= \sum_{j=1}^{\text{n}} e_{j,x}\left\{\int_\Omega \frac{\partial}{\partial x}S(\chi_{\text{e}}\phi_{j,x})\frac{\partial}{\partial y}\eta_{i,y}\mathrm{d}\Omega - \int_{\partial\Omega}\eta_{i,y}\frac{\partial}{\partial x}S(\chi_{\text{e}}\phi_{j,x})\mathrm{d}\Gamma\right\} \\
&\quad + \sum_{j=1}^{\text{n}} e_{j,y}\left\{\int_\Omega \phi_{j,y}\eta_{i,y}\mathrm{d}\Omega + \xi_0\eta_0\int_\Omega S(\chi_{\text{e}}\phi_{j,y})\eta_{i,y}\mathrm{d}\Omega\right. \\
&\quad \left. + \int_\Omega \frac{\partial}{\partial y}S(\chi_{\text{e}}\phi_{j,y})\frac{\partial}{\partial y}\eta_{i,y}\mathrm{d}\Omega - \int_{\partial\Omega}\eta_{i,y}\frac{\partial}{\partial y}S(\chi_{\text{e}}\phi_{j,y})\mathrm{d}\Gamma\right\} \qquad i = 1,..,\text{n}.
\end{aligned}$$

Note that the expansion of the electric field in the first weak form results in volume integrals only, whereas the expansion of the electric field in the second weak form results in volume integrals and boundary integrals.

3.2.2. EXPANDING BOTH THE ELECTRIC FIELD AND THE VECTOR POTENTIAL

Substitution of $\hat{E}_x^{\mathrm{n}}$, $\hat{E}_y^{\mathrm{n}}$, $S^{\mathrm{n}}(\chi_{\mathrm{e}}\hat{E}_x)$ and $S^{\mathrm{n}}(\chi_{\mathrm{e}}\hat{E}_y)$ in (3.3) and (3.4) results in

$$\begin{aligned}
\int_\Omega \hat{E}_x^{\mathrm{inc}}\eta_{i,x}\mathrm{d}\Omega &= \sum_{j=1}^{\mathrm{n}} e_{j,x}\left\{\int_\Omega \phi_{j,x}\eta_{i,x}\mathrm{d}\Omega\right\} \\
&\quad + \sum_{j=1}^{\mathrm{n}} s_{j,x}\left\{\xi_0\eta_0\int_\Omega \phi_{j,x}\eta_{i,x}\mathrm{d}\Omega - \int_\Omega \eta_{i,x}\frac{\partial}{\partial x}\frac{\partial}{\partial x}\phi_{j,x}\mathrm{d}\Omega\right\} \\
&\quad - \sum_{j=1}^{\mathrm{n}} s_{j,y}\left\{\int_\Omega \eta_{i,x}\frac{\partial}{\partial x}\frac{\partial}{\partial y}\phi_{j,y}\mathrm{d}\Omega\right\} \qquad i = 1,..,\mathrm{n} \qquad (3.7)\\
\int_\Omega \hat{E}_y^{\mathrm{inc}}\eta_{i,y}\mathrm{d}\Omega &= \sum_{j=1}^{\mathrm{n}} e_{j,y}\left\{\int_\Omega \phi_{j,y}\eta_{i,y}\mathrm{d}\Omega\right\} \\
&\quad - \sum_{j=1}^{\mathrm{n}} s_{j,x}\left\{\int_\Omega \eta_{i,y}\frac{\partial}{\partial y}\frac{\partial}{\partial x}\phi_{j,x}\mathrm{d}\Omega\right\} \\
&\quad + \sum_{j=1}^{\mathrm{n}} s_{j,y}\left\{\xi_0\eta_0\int_\Omega \phi_{j,y}\eta_{i,y}\mathrm{d}\Omega - \int_\Omega \eta_{i,y}\frac{\partial}{\partial y}\frac{\partial}{\partial y}\phi_{j,y}\mathrm{d}\Omega\right\} \qquad i = 1,..,\mathrm{n}. \qquad (3.8)
\end{aligned}$$

Also, substitution of $\hat{E}_x^{\mathrm{n}}$, $\hat{E}_y^{\mathrm{n}}$, $S^{\mathrm{n}}(\chi_{\mathrm{e}}\hat{E}_x)$ and $S^{\mathrm{n}}(\chi_{\mathrm{e}}\hat{E}_y)$ in (3.5) and (3.6) results in

$$\begin{aligned}
\int_\Omega \hat{E}_x^{\mathrm{inc}}\eta_{i,x}\mathrm{d}\Omega &= \sum_{j=1}^{\mathrm{n}} e_{j,x}\left\{\int_\Omega \phi_{j,x}\eta_{i,x}\mathrm{d}\Omega\right\} \\
&\quad + \sum_{j=1}^{\mathrm{n}} s_{j,x}\left\{\xi_0\eta_0\int_\Omega \phi_{j,x}\eta_{i,x}\mathrm{d}\Omega + \int_\Omega \frac{\partial}{\partial x}\phi_{j,x}\frac{\partial}{\partial x}\eta_{i,x}\mathrm{d}\Omega - \int_{\partial\Omega} \eta_{i,x}\frac{\partial}{\partial x}\phi_{j,x}\mathrm{d}\Gamma\right\} \\
&\quad + \sum_{j=1}^{\mathrm{n}} s_{j,y}\left\{\int_\Omega \frac{\partial}{\partial y}\phi_{j,y}\frac{\partial}{\partial x}\eta_{i,x}\mathrm{d}\Omega - \int_{\partial\Omega} \eta_{i,x}\frac{\partial}{\partial y}\phi_{j,y}\mathrm{d}\Gamma\right\} \qquad i = 1,..,\mathrm{n} \qquad (3.9)\\
\int_\Omega \hat{E}_y^{\mathrm{inc}}\eta_{i,y}\mathrm{d}\Omega &= \sum_{j=1}^{\mathrm{n}} e_{j,y}\left\{\int_\Omega \phi_{j,y}\eta_{i,y}\mathrm{d}\Omega\right\} \\
&\quad + \sum_{j=1}^{\mathrm{n}} s_{j,x}\left\{\int_\Omega \frac{\partial}{\partial x}\phi_{j,x}\frac{\partial}{\partial y}\eta_{i,y}\mathrm{d}\Omega - \int_{\partial\Omega} \eta_{i,y}\frac{\partial}{\partial x}\phi_{j,x}\mathrm{d}\Gamma\right\} \qquad i = 1,..,\mathrm{n} \\
&\quad + \sum_{j=1}^{\mathrm{n}} s_{j,y}\left\{\xi_0\eta_0\int_\Omega \phi_{j,y}\eta_{i,y}\mathrm{d}\Omega + \int_\Omega \frac{\partial}{\partial y}\phi_{j,y}\frac{\partial}{\partial y}\eta_{i,y}\mathrm{d}\Omega - \int_{\partial\Omega} \eta_{i,y}\frac{\partial}{\partial y}\phi_{j,y}\mathrm{d}\Gamma\right\}. \qquad (3.10)
\end{aligned}$$

The coefficients $e_{j,x}$ and $s_{j,x}$ are related, just like the coefficients $e_{j,y}$ and $s_{j,y}$, via

$$\sum_{j=1}^{\mathrm{n}} s_{j,\alpha}\phi_{j,\alpha}(\mathbf{x}) = S^{\mathrm{n}}(\chi_{\mathrm{e}}\hat{E}_\alpha)(\mathbf{x}) \approx \int_{x'} \hat{g}(\mathbf{x}-\mathbf{x}')\chi_{\mathrm{e}}(\mathbf{x}')\hat{E}_\alpha(\mathbf{x}')\mathrm{d}V' \approx \int_{x'} \hat{g}(\mathbf{x}-\mathbf{x}')\chi_{\mathrm{e}}(\mathbf{x}')\sum_{j=1}^{\mathrm{n}} e_{j,\alpha}\phi_{j,\alpha}(\mathbf{x}')\mathrm{d}V'. \qquad (3.11)$$

In some approaches where both the electric field and the vector potential have been expanded, one can make use of the fact that the vector potential is a convolution of the Green's function and the product of the contrast function and the electric field. The result of a convolution can easily be calculated with Fast Fourier Transforms. The big advantage is that the Green's function only has to be calculated in all the grid nodes once instead of in all possible combinations of differences between two grid points, as one would expect. An example of a formulation in which this is possible will be shown in Section 3.5.

After both of the expansion procedures the resulting equations can be written as a system of size $2\mathrm{n}\times 2\mathrm{n}$ of the form

$$\begin{bmatrix} A^{\mathrm{a}} & A^{\mathrm{b}} \\ A^{\mathrm{c}} & A^{\mathrm{d}} \end{bmatrix}\begin{bmatrix} \mathbf{e}^{\mathrm{a}} \\ \mathbf{e}^{\mathrm{b}} \end{bmatrix} = \begin{bmatrix} \mathbf{f}^{\mathrm{a}} \\ \mathbf{f}^{\mathrm{b}} \end{bmatrix} \qquad (3.12)$$

where the elements of the submatrices $\mathbf{e}^{\mathrm{a}}$ and $\mathbf{e}^{\mathrm{b}}$ are defined by

$$\begin{aligned} e_j^{\mathrm{a}} &= e_{j,x} \qquad j = 1,..,\mathrm{n} \\ e_j^{\mathrm{b}} &= e_{j,y} \qquad j = 1,..,\mathrm{n} \end{aligned}$$

and the elements of the subvectors $\mathbf{f}^{\mathrm{a}}$ and $\mathbf{f}^{\mathrm{b}}$ by

$$\begin{aligned} f_i^{\mathrm{a}} &= \int_\Omega \hat{E}_x^{\mathrm{inc}} \phi_{i,x} \mathrm{d}\Omega \qquad i = 1,..,\mathrm{n} \\ f_i^{\mathrm{b}} &= \int_\Omega \hat{E}_y^{\mathrm{inc}} \phi_{i,y} \mathrm{d}\Omega \qquad i = 1,..,\mathrm{n}. \end{aligned}$$

The elements of the submatrices A^{a}, A^{b}, A^{c} and A^{d} depend on the choice of basis and test functions and on the weak formulation.

3.3. CHOICE OF BASIS AND TEST FUNCTIONS

There are numerous possibilities to choose the basis and test functions. Two choices of test functions are popular and result in different techniques: the Point Callocation Method and Galerkin's Method. Below both of the methods will be discussed.
When constructing the test and basis functions, it is useful to keep in mind the type of function that needs to be approximated. A continuous function can be approximated with continuous or discontinuous basis functions. A discontinuous function, however, is in general better approximated with discontinuous basis functions.

3.3.1. GALERKIN'S METHOD

In Galerkin's method the test functions are chosen to be the same as the basis functions, so $\eta_x = \phi_{i,x}$ and $\eta_y = \phi_{i,y}$ for $i = 1,..,\mathrm{n}$. The resulting equations

$$\begin{aligned} \int_\Omega \hat{E}_x^{\mathrm{inc}} \phi_{i,x} \mathrm{d}\Omega &= \sum_{j=1}^{\mathrm{n}} e_{j,x} \left\{ \int_\Omega \phi_{j,x} \phi_{i,x} \mathrm{d}\Omega + \xi_0 \eta_0 \int_\Omega S(\chi_{\mathrm{e}} \phi_{j,x}) \phi_{i,x} \mathrm{d}\Omega + \int_\Omega \frac{\partial}{\partial x} S(\chi_{\mathrm{e}} \phi_{j,x}) \frac{\partial}{\partial x} \phi_{i,x} \mathrm{d}\Omega \right. \\ &\quad \left. - \int_{\partial\Omega} \frac{\partial}{\partial x} S(\chi_{\mathrm{e}} \phi_{j,x}) \phi_{i,x} \mathrm{d}\Gamma \right\} \\ &\quad + \sum_{j=1}^{\mathrm{n}} e_{j,y} \left\{ \int_\Omega \frac{\partial}{\partial y} S(\chi_{\mathrm{e}} \phi_{j,y}) \frac{\partial}{\partial x} \phi_{i,x} \mathrm{d}\Omega - \int_{\partial\Omega} \frac{\partial}{\partial y} S(\chi_{\mathrm{e}} \phi_{j,y}) \phi_{i,x} \mathrm{d}\Gamma \right\}, \qquad i = 1,..,\mathrm{n} \\ \int_\Omega \hat{E}_y^{\mathrm{inc}} \phi_{i,y} \mathrm{d}\Omega &= \sum_{j=1}^{\mathrm{n}} e_{j,y} \left\{ \int_\Omega \phi_{j,y} \phi_{i,y} \mathrm{d}\Omega + \xi_0 \eta_0 \int_\Omega S(\chi_{\mathrm{e}} \phi_{j,y}) \phi_{i,y} \mathrm{d}\Omega + \int_\Omega \frac{\partial}{\partial y} S(\chi_{\mathrm{e}} \phi_{j,y}) \frac{\partial}{\partial y} \phi_{i,y} \mathrm{d}\Omega \right. \\ &\quad \left. - \int_{\partial\Omega} \frac{\partial}{\partial y} S(\chi_{\mathrm{e}} \phi_{j,y}) \phi_{i,y} \mathrm{d}\Gamma \right\} \\ &\quad + \sum_{j=1}^{\mathrm{n}} e_{j,x} \left\{ \int_\Omega \frac{\partial}{\partial x} S(\chi_{\mathrm{e}} \phi_{j,x}) \frac{\partial}{\partial y} \phi_{i,y} \mathrm{d}\Omega - \int_{\partial\Omega} \frac{\partial}{\partial x} S(\chi_{\mathrm{e}} \phi_{j,x}) \phi_{i,y} \mathrm{d}\Gamma \right\}, \qquad i = 1,..,\mathrm{n}. \end{aligned}$$

define the system in which the submatrices A^{a}, A^{b}, A^{c} and A^{d} in (3.12) are defined by

$$\begin{aligned} A_{ij}^{\mathrm{a}} &= \int_\Omega \phi_{j,x} \phi_{i,x} \mathrm{d}\Omega + \xi_0 \eta_0 \int_\Omega S(\chi_{\mathrm{e}} \phi_{j,x}) \phi_{i,x} \mathrm{d}\Omega + \int_\Omega \tfrac{\partial}{\partial x} S(\chi_{\mathrm{e}} \phi_{j,x}) \tfrac{\partial}{\partial x} \phi_{i,x} \mathrm{d}\Omega - \int_{\partial\Omega} \tfrac{\partial}{\partial x} S(\chi_{\mathrm{e}} \phi_{j,x}) \phi_{i,x} \mathrm{d}\Gamma \qquad i,j = 1,..,\mathrm{n} \\ A_{ij}^{\mathrm{b}} &= \int_\Omega \tfrac{\partial}{\partial y} S(\chi_{\mathrm{e}} \phi_{j,y}) \tfrac{\partial}{\partial x} \phi_{i,x} \mathrm{d}\Omega - \int_{\partial\Omega} \tfrac{\partial}{\partial y} S(\chi_{\mathrm{e}} \phi_{j,y}) \phi_{i,x} \mathrm{d}\Gamma \qquad i,j = 1,..,\mathrm{n} \\ A_{ij}^{\mathrm{c}} &= \int_\Omega \tfrac{\partial}{\partial x} S(\chi_{\mathrm{e}} \phi_{j,x}) \tfrac{\partial}{\partial y} \phi_{i,y} \mathrm{d}\Omega - \int_{\partial\Omega} \tfrac{\partial}{\partial x} S(\chi_{\mathrm{e}} \phi_{j,x}) \phi_{i,y} \mathrm{d}\Gamma \qquad i,j = 1,..,\mathrm{n} \\ A_{ij}^{\mathrm{d}} &= \int_\Omega \phi_{j,y} \phi_{i,y} \mathrm{d}\Omega + \xi_0 \eta_0 \int_\Omega S(\chi_{\mathrm{e}} \phi_{j,y}) \phi_{i,y} \mathrm{d}\Omega + \int_\Omega \tfrac{\partial}{\partial y} S(\chi_{\mathrm{e}} \phi_{j,y}) \tfrac{\partial}{\partial y} \phi_{i,y} \mathrm{d}\Omega - \int_{\partial\Omega} \tfrac{\partial}{\partial y} S(\chi_{\mathrm{e}} \phi_{j,y}) \phi_{i,y} \mathrm{d}\Gamma \qquad i,j = 1,..,\mathrm{n}. \end{aligned}$$

3.3.2. POINT CALLOCATION METHOD

In the Point Callocation Method the test functions are chosen to be the dirac delta functions, $\eta_{x,i} = \delta(x - x_i)$ for $i = 1,..,\mathrm{n}$. This means that the weak form that was used in Galerkin's method would give problems here, because the derivative of the dirac delta function would appear in the formulation. Therefore the first weak form is used to demonstrate the Point Callocation Method.

$$\begin{aligned}
\hat{E}_x^{\text{inc}}(\mathbf{x}_i) &= \sum_{j=1}^{\text{n}} e_{j,x}\left\{\phi_{j,x}(\mathbf{x}_i)+\xi_0\eta_0 S(\chi_{\text{e}}\phi_{j,x})(\mathbf{x}_i)-\frac{\partial}{\partial x}\frac{\partial}{\partial x}S(\chi_{\text{e}}\phi_{j,x})(\mathbf{x}_i)\right\} \\
&\quad -\sum_{j=1}^{\text{n}} e_{j,y}\left\{\frac{\partial}{\partial x}\frac{\partial}{\partial y}S(\chi_{\text{e}}\phi_{j,y})(\mathbf{x}_i)\right\} \qquad i=1,..,\text{n} \\
\hat{E}_y^{\text{inc}}(\mathbf{x}_i) &= \sum_{j=1}^{\text{n}} e_{j,y}\left\{\phi_{j,y}(\mathbf{x}_i)+\xi_0\eta_0 S(\chi_{\text{e}}\phi_{j,y})(\mathbf{x}_i)-\frac{\partial}{\partial y}\frac{\partial}{\partial y}S(\chi_{\text{e}}\phi_{j,x})(\mathbf{x}_i)\right\} \\
&\quad -\sum_{j=1}^{\text{n}} e_{j,x}\left\{\frac{\partial}{\partial y}\frac{\partial}{\partial x}S(\chi_{\text{e}}\phi_{j,x})(\mathbf{x}_i)\right\} \qquad i=1,..,\text{n}.
\end{aligned}$$

define the system in which the submatrices $A^{\text{a}}, A^{\text{b}}, A^{\text{c}}$ and A^{d} in (3.12) are defined by

$$\begin{aligned}
A_{ij}^{\text{a}} &= \phi_{j,x}(\mathbf{x}_i)+\xi_0\eta_0 S(\chi_{\text{e}}\phi_{j,x})(\mathbf{x}_i)-\tfrac{\partial}{\partial x}\tfrac{\partial}{\partial x}S(\chi_{\text{e}}\phi_{j,x})(\mathbf{x}_i) && i,j=1,..,\text{n} \\
A_{ij}^{\text{b}} &= -\tfrac{\partial}{\partial x}\tfrac{\partial}{\partial y}S(\chi_{\text{e}}\phi_{j,y})(\mathbf{x}_i) && i,j=1,..,\text{n} \\
A_{ij}^{\text{c}} &= -\tfrac{\partial}{\partial y}\tfrac{\partial}{\partial x}S(\chi_{\text{e}}\phi_{j,x})(\mathbf{x}_i) && i,j=1,..,\text{n} \\
A_{ij}^{\text{d}} &= \phi_{j,y}(\mathbf{x}_i)+\xi_0\eta_0 S(\chi_{\text{e}}\phi_{j,y})(\mathbf{x}_i)-\tfrac{\partial}{\partial y}\tfrac{\partial}{\partial y}S(\chi_{\text{e}}\phi_{j,y})(\mathbf{x}_i) && i,j=1,..,\text{n}.
\end{aligned}$$

The choice of test functions makes the integral over the domain of the test functions disappear. This is computationally more efficient than Galerkin's Method, where the integration over the domain of the test function often results in extra matrices that connect neighbouring elements. However, a drawback of the Point Callocation Method is that the test function does not take into account the boundary conditions that were discribed in Section 2.2, whereas in Galerkin's Method it is possible to choose the basis functions so that they do take into account the boundary conditions.

3.4. EXAMPLE: TRIANGULAR MESH WITH LINEAR BASIS FUNCTIONS

In order to find the elements of the matrix A, the integrals over the domain Ω are written as a sum of integrals over small subdomains, called elements e. By first integrating the expressions over small subdomains, numerical integration rules can be used to simplify the calculations. In this report the domain is devided into triangles and linear basis functions are defined on each triangle. In total there are n basis functions for each component,

$$\begin{aligned}
\phi_{i,x}(\mathbf{x}) &= \alpha_{i,x}+\beta_{i,x}x+\gamma_{i,x}y && i=1,..,n \\
\phi_{i,y}(\mathbf{x}) &= \alpha_{i,y}+\beta_{i,y}x+\gamma_{i,y}y && i=1,..,n,
\end{aligned}$$

satisfying $\phi_{i,x}(\mathbf{x}_j)=\delta_{ij}$ and $\phi_{i,y}(\mathbf{x}_j)=\delta_{ij}$, so that the i'th basis function behaves as shown in Figure 3.1. The actual form of the basis functions is determined by the coefficients $\alpha_{i,x},\beta_{i,x}$ and $\gamma_{i,x}$ for the basis function in the x-direction and $\alpha_{i,y},\beta_{i,y}$ and $\gamma_{i,y}$ for the basis function in the y-direction. On each triangle there exist three basis functions that satisfy the delta property in the three vertices. Therefore the coefficients for the $x-$directional basis functions $\phi_{1,x},\phi_{2,x}$ and $\phi_{3,x}$ on triangle e follow from the system

$$\begin{bmatrix}1 & x_1 & y_1\\ 1 & x_2 & y_2\\ 1 & x_3 & y_3\end{bmatrix}\begin{bmatrix}\alpha_{1,x} & \beta_{1,x} & \gamma_{1,x}\\ \alpha_{2,x} & \beta_{2,x} & \gamma_{2,x}\\ \alpha_{3,x} & \beta_{3,x} & \gamma_{3,x}\end{bmatrix}=\begin{bmatrix}1 & 0 & 0\\ 0 & 1 & 0\\ 0 & 0 & 1\end{bmatrix}$$

where $(x_1,y_1),(x_2,y_2)$ and (x_3,y_3) are the vertices of one element. The same procedure also gives the coefficients for the y-directional basis functions.

An important theorem used to deal with the integration of (a product of) linear basis functions over a triangular element is named as Holand & Bell's thorem.

Theorem 1. *Let e be a triangle in $\mathbb{R}^2$ with vertices $\mathbf{x}_1,\mathbf{x}_2,\mathbf{x}_3$ and let $\lambda_1,\lambda_2\lambda_3$ on e be linear on e. Further, let $\lambda_i(x_j,y_j)=\delta_{ij}$ and finally let $m_1,m_2,m_3\in\mathbb{N}$. Then, $\int_e \lambda_1^{m_1}\lambda_2^{m_2}\lambda_3^{m_3}\,d\Omega=\frac{|\Delta|m_1!m_2!m_3!}{(2+m_1+m_2+m_3)!}$, where $|\Delta|$ is two times the area of e.*

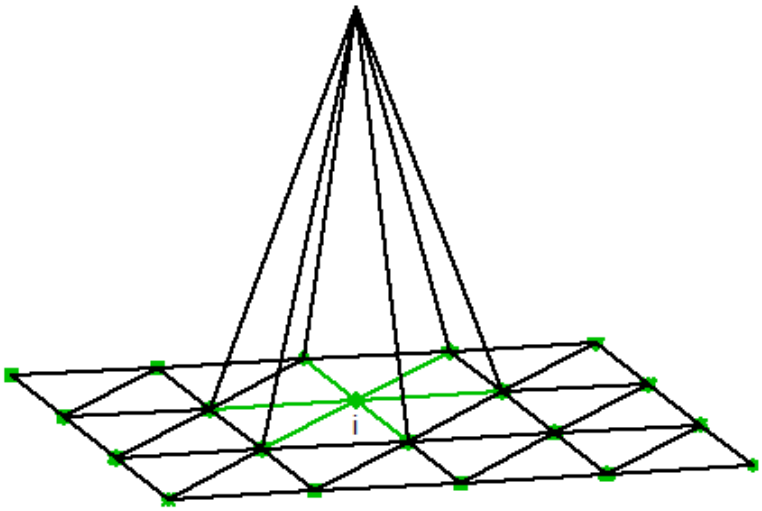

Figure 3.1: Basis function number i

The first approximation where Holand & Bell's theorem is used is

$$\int_e \phi_{j,x}\phi_{i,x}\mathrm{d}\Omega_e \overset{\text{Holand \& Bell}}{\approx} \frac{|\Delta|}{24}(1+\delta_{ij}) \qquad i,j=1,2,3$$
$$\int_e \phi_{j,y}\phi_{i,y}\mathrm{d}\Omega_e \overset{\text{Holand \& Bell}}{\approx} \frac{|\Delta|}{24}(1+\delta_{ij}) \qquad i,j=1,2,3$$

where it is important to note that i and j run in this special case over the vertices of element e, because the product of the i'th and j'th basis functions vanish if one or both of nodes i and j are located outside element e. A bit more complicated approximation follows from

$$\begin{aligned}
\xi_0\eta_0\int_e S(\chi_e\phi_{j,x})\phi_{i,x}\mathrm{d}\Omega_e &\overset{\text{Interpolation}}{\approx} \xi_0\eta_0\textstyle\int_e\sum_{p=1,2,3} S(\chi_e\phi_{j,x})(\mathbf{x}_p)\phi_{i,x}(\mathbf{x}_p)\lambda_p(\mathbf{x})\mathrm{d}\Omega_e && i=1,2,3 \quad j=1,..,n\\
&= \xi_0\eta_0\textstyle\sum_{p=1,2,3} S(\chi_e\phi_{j,x})(\mathbf{x}_p)\phi_{i,x}(\mathbf{x}_p)\int_e\lambda_p(\mathbf{x})\mathrm{d}\Omega_e && i=1,2,3 \quad j=1,..,n\\
&\overset{\text{Holand \& Bell}}{=} \xi_0\eta_0\textstyle\sum_{p=1,2,3} S(\chi_e\phi_{j,x})(\mathbf{x}_p)\phi_{i,x}(\mathbf{x}_p)\frac{|\Delta|}{6} && i=1,2,3 \quad j=1,..,n\\
&\overset{\phi_{i,x}(\mathbf{x}_p)=\delta_{ip}}{=} \xi_0\eta_0 S(\chi_e\phi_{j,x})(\mathbf{x}_i)\frac{|\Delta|}{6} && i=1,2,3 \quad j=1,..,n\\
\xi_0\eta_0\int_e S(\chi_e\phi_{j,y})\phi_{i,y}\mathrm{d}\Omega_e \approx &\ \xi_0\eta_0 S(\chi_e\phi_{j,y})(\mathbf{x}_i)\frac{|\Delta|}{6} && i=1,2,3 \quad j=1,..,n.
\end{aligned}$$

The i'th basis function vanishes if node i is located outside tirangle e, whereas the function $S(\chi_e\phi_{j,y})$ is defined on all nodes. Therefore i runs over the vertices of triangle e and j runs over all nodes. Also p runs over the vertices of the triangle.

Next, the derivative terms are approximated as

$$\begin{aligned}
\int_e \frac{\partial}{\partial x} S(\chi_e \phi_{j,x}) \frac{\partial}{\partial x} \phi_{i,x} \mathrm{d}\Omega_e &\overset{\frac{\partial}{\partial x}\phi_{i,x}=\beta_{i,x}}{=} && \beta_{i,x} \int_e \tfrac{\partial}{\partial x} S(\chi_e \phi_{j,x}) \mathrm{d}\Omega_e && i=1,2,3 && j=1,..,n \\
&\overset{\text{Interpolation}}{\approx} && \beta_{i,x} \int_e \textstyle\sum_{p=1,2,3} \tfrac{\partial}{\partial x} S(\chi_e \phi_{j,x})(\mathbf{x}_p) \lambda_p(\mathbf{x}) \mathrm{d}\Omega_e && i=1,2,3 && j=1,..,n \\
&= && \beta_{i,x} \textstyle\sum_{p=1,2,3} \tfrac{\partial}{\partial x} S(\chi_e \phi_{j,x})(\mathbf{x}_p) \int_e \lambda_p(\mathbf{x}) \mathrm{d}\Omega_e && i=1,2,3 && j=1,..,n \\
&= && \beta_{i,x} \textstyle\sum_{p=1,2,3} \tfrac{\partial}{\partial x} S(\chi_e \phi_{j,x})(\mathbf{x}_p) \tfrac{|\Delta|}{6} && i=1,2,3 && j=1,..,n \\
\int_e \frac{\partial}{\partial y} S(\chi_e \phi_{j,y}) \frac{\partial}{\partial y} \phi_{i,y} \mathrm{d}\Omega_e &\overset{\frac{\partial}{\partial y}\phi_{i,y}=\gamma_{i,y}}{=} && \gamma_{i,y} \textstyle\sum_{p=1,2,3} \tfrac{\partial}{\partial y} S(\chi_e \phi_{j,y})(\mathbf{x}_p) \tfrac{|\Delta|}{6} && i=1,2,3 && j=1,..,n \\
\int_e \frac{\partial}{\partial y} S(\chi_e \phi_{j,y}) \frac{\partial}{\partial x} \phi_{i,x} \mathrm{d}\Omega_e &\overset{\frac{\partial}{\partial x}\phi_{i,x}=\beta_{i,x}}{=} && \beta_{i,x} \textstyle\sum_{p=1,2,3} \tfrac{\partial}{\partial y} S(\chi_e \phi_{j,y})(\mathbf{x}_p) \tfrac{|\Delta|}{6} && i=1,2,3 && j=1,..,n \\
\int_e \frac{\partial}{\partial x} S(\chi_e \phi_{j,x}) \frac{\partial}{\partial y} \phi_{i,y} \mathrm{d}\Omega_e &\overset{\frac{\partial}{\partial y}\phi_{i,y}=\gamma_{i,y}}{=} && \gamma_{i,y} \textstyle\sum_{p=1,2,3} \tfrac{\partial}{\partial x} S(\chi_e \phi_{j,x})(\mathbf{x}_p) \tfrac{|\Delta|}{6} && i=1,2,3 && j=1,..,n
\end{aligned}$$

where again the derivative of the i'th basis function vanishes if node i is located outside element e and therefore i runs over the vertices of triangle e and j runs over all nodes.

Finally,

$$\begin{aligned}
\int_{\partial e} \frac{\partial}{\partial x} S(\chi_e \phi_{j,x}) \phi_{i,x} \mathrm{d}\Gamma_e &\overset{\text{Interpolation}}{\approx} && \textstyle\int_{\partial e} \sum_{p=1,2} \tfrac{\partial}{\partial x} S(\chi_e \phi_{j,x})(\mathbf{x}_p) \phi_{i,x}(\mathbf{x}_p) \lambda_p(\mathbf{x}) \mathrm{d}\Gamma_e && i=1,2 && j=1,..,n \\
&= && \textstyle\sum_{p=1,2} \tfrac{\partial}{\partial x} S(\chi_e \phi_{j,x})(\mathbf{x}_p) \phi_{i,x}(\mathbf{x}_p) \int_{\partial e} \lambda_p(\mathbf{x}) \mathrm{d}\Gamma_e && i=1,2 && j=1,..,n \\
&\overset{\phi_{i,x}(\mathbf{x}_p)=\delta_{ip}}{=} && \tfrac{\partial}{\partial x} S(\chi_e \phi_{j,x})(\mathbf{x}_i) \textstyle\int_{\partial e} \lambda_p(\mathbf{x}) \mathrm{d}\Gamma_e && i=1,2 && j=1,..,n \\
&\overset{\text{Holand \& Bell}}{\approx} && \tfrac{\partial}{\partial x} S(\chi_e \phi_{j,x})(\mathbf{x}_i) \tfrac{||\mathbf{x}_k - \mathbf{x}_l||}{2} && i=1,2 && j=1,..,n \\
\int_{\partial e} \frac{\partial}{\partial y} S(\chi_e \phi_{j,y}) \phi_{i,x} \mathrm{d}\Gamma_e &\approx && \tfrac{\partial}{\partial y} S(\chi_e \phi_{j,y})(\mathbf{x}_i) \tfrac{||\mathbf{x}_k - \mathbf{x}_l||}{2} && i=1,2 && j=1,..,n \\
\int_{\partial e} \frac{\partial}{\partial x} S(\chi_e \phi_{j,x}) \phi_{i,y} \mathrm{d}\Gamma_e &\approx && \tfrac{\partial}{\partial x} S(\chi_e \phi_{j,x})(\mathbf{x}_i) \tfrac{||\mathbf{x}_k - \mathbf{x}_l||}{2} && i=1,2 && j=1,..,n \\
\int_{\partial e} \frac{\partial}{\partial y} S(\chi_e \phi_{j,y}) \phi_{i,y} \mathrm{d}\Gamma_e &\approx && \tfrac{\partial}{\partial y} S(\chi_e \phi_{j,y})(\mathbf{x}_i) \tfrac{||\mathbf{x}_k - \mathbf{x}_l||}{2} && i=1,2 && j=1,..,n
\end{aligned}$$

where i runs over the endpoints of line e and j runs over all nodes. The indices k and l correspond to the two endpoints of line e. In practice, however, the contrast is set to zero at the boundary of Ω and therefore the contributions of all boundary elements vanish.

In all these approximated terms, there still is a term that needs some more explanation. The term $S(\chi_e \phi_{j,x})$ is a function of $\mathbf{x}$ that contains an integral over the entire domain. However, the fact that the j'th basis function has a compact support makes the calculations easier. More specifically, the support of basis function j only contains points lying in the triangles that have node j as a vertex. The following derivation shows the simplification of the integral term for an internal node j.

$$\begin{aligned}
S(\chi_e \phi_{j,x})(\mathbf{x}) &= \int_\Omega \hat{g}(\mathbf{x}-\mathbf{x}', s) \chi_e(\mathbf{x}') \phi_{j,x}(\mathbf{x}') \mathrm{d}V' \\
&= \int_{\mathrm{supp}(\phi_{j,x})} \hat{g}(\mathbf{x}-\mathbf{x}', s) \chi_e(\mathbf{x}') \phi_{j,x}(\mathbf{x}') \mathrm{d}V' \\
&= \int_{e_{j_1}} \hat{g}(\mathbf{x}-\mathbf{x}', s) \chi_e(\mathbf{x}') \phi_{j,x}(\mathbf{x}') \mathrm{d}V' + \cdots + \int_{e_{j_6}} \hat{g}(\mathbf{x}-\mathbf{x}', s) \chi_e(\mathbf{x}') \phi_{j,x}(\mathbf{x}') \mathrm{d}V' \\
&\overset{\text{Interpolation}}{=} \sum_{p=1,2,3} \hat{g}(\mathbf{x}-\mathbf{x}_p, s) \chi_e(\mathbf{x}_p) \delta_{jp} \frac{|\Delta|}{6} + \cdots + \sum_{q=1,2,3} \hat{g}(\mathbf{x}-\mathbf{x}_q, s) \chi_e(\mathbf{x}_q) \delta_{jq} \frac{|\Delta|}{6} \\
&= \hat{g}(\mathbf{x}-\mathbf{x}_j, s) \chi_e(\mathbf{x}_j) \frac{|\Delta|}{6} + \cdots + \hat{g}(\mathbf{x}-\mathbf{x}_j, s) \chi_e(\mathbf{x}_j) \frac{|\Delta|}{6} \\
&= \hat{g}(\mathbf{x}-\mathbf{x}_j, s) \chi_e(\mathbf{x}_j) |\Delta| \qquad (3.13)
\end{aligned}$$

The same result would have been obtained if the integral was approximated by using the Midpoint rule and the delta property. For nodes that lie on the boundary (3.13) has to be multiplied with a factor $NT/6$, where NT is the number of triangles in which node j is a vertex.
Now that (3.13) is found, the spatial derivatives of $S(\chi_e\phi_{j,x})$ can be calculated directly by differentiating the Green's function. In Chapter B the singularity in the Green's function will be dealt with.

VECTOR AND MATRIX ASSEMBLY

In the assembling part the total system matrix is constructed. The term $\int_e \phi_{j,x}\phi_{i,x}d\Omega_e$ contributes to a maximum of seven diagonals in the system matrix, because each node is present in six surrounding triangles that all have two other vertices. The other terms make the system matrix a full matrix (in case of nonzero contrast everywhere) because of the vector potential present in each of the terms. Figure 3.2 shows the sparsity pattern of the final system matrix in case of 32 triangular elements (25 nodes). Filled column j corresponds with node j that has nonzero contrast. In this case only six nodes have nonzero contrast.

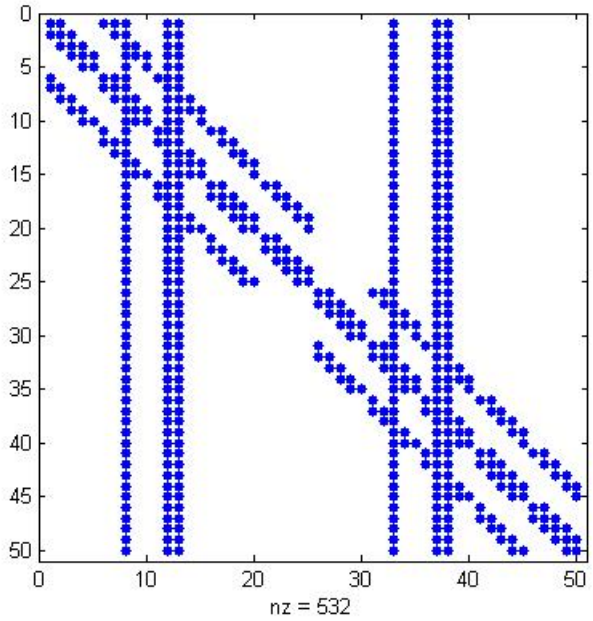

Figure 3.2: Sparsity pattern of the system matrix with 32 triangular elements.

3.5. EXAMPLE: RECTANGULAR MESH WITH ROOFTOP BASIS FUNCTIONS

Another way of solving the volume integral equation is using rectangular elements, with each node lying in the center of a rectangular element. Basis functions ϕ_{mn} and test functions ϕ_{pq} are defined on each node such that the basis functions are linear in one direction and constant in the other direction for a specified region. Galerkin's Method is used, so the basis functions are chosen the same as the test functions. The starting point in this example is the second weak form, but next to expanding the electric field and the vector potential, also the electric incident field is expanded. In case of simple basis functions one could also choose for analytically calculating the weighting on the incident field without expanding it.
It is important to note that in (3.9) a first derivative with respect to the x-direction acts on the x-directional basis function and on the x-directional test function, and a first derivative with respect to the y-direction acts on the y-directional basis function and on the y-directional test function. The same holds for (3.10). For this reason, the basis functions for the x-component should be piecewise differentiable with respect to x and the basis functions for the y-component should be piecewise differentiable with respect to y. Basis functions that satisfy this condition are

$$\phi^x_{mn} = \Lambda_m(x)\Pi_n(y)$$

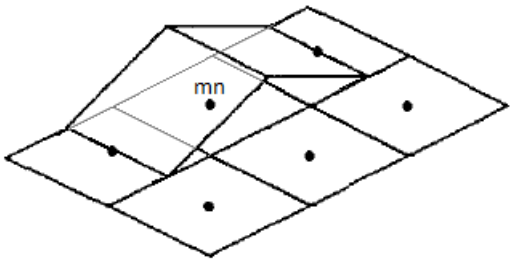

Figure 3.3: Basis function corresponding to node mn

for the x component and

$$\phi^{y}_{mn} \quad = \quad \Pi_n(x)\Lambda_m(y)$$

for the y component, where

$$\Lambda_m(x) = \begin{cases} 1 - \frac{1}{\Delta x}|x - x_m| & |x - x_m| \leq \Delta x \\ 0 & |x - x_m| > \Delta x \end{cases}$$

and

$$\Pi_n(y) = \begin{cases} 1 & y_{n-\frac{1}{2}} < y < y_{n+\frac{1}{2}} \\ \frac{1}{2} & y = y_{n-\frac{1}{2}} \bigvee y = y_{n+\frac{1}{2}} \\ 0 & y > y_{n-\frac{1}{2}} \bigvee y > y_{n+\frac{1}{2}} \end{cases}.$$

Figure 3.3 shows the behaviour of the basis function corresponding to node m, n.

With the help of these basis functions the weighting procedure can be performed. In this example three equations that have to be taken into account:

- $\hat{\mathbf{E}}^{\text{inc}} = \hat{\mathbf{E}} + (\xi_0\eta_0 - \nabla\nabla\cdot)\,\mathbf{S}(\hat{\mathbf{J}})$
- $\mathbf{S}(\hat{\mathbf{J}}) = \int_{\mathbf{x}'} \hat{g}(\mathbf{x}-\mathbf{x}')\hat{\mathbf{J}}d\mathbf{x}'$
- $\hat{\mathbf{J}} = \chi_e\hat{\mathbf{E}}$.

The corresponding expansions are

$$\hat{E}_\alpha \approx \sum_m \sum_n e^{\alpha}_{mn}\phi^{\alpha}_{mn},$$

$$S_\alpha \approx \sum_m \sum_n s^{\alpha}_{mn}\phi^{\alpha}_{mn},$$

$$\hat{J}_\alpha \approx \sum_m \sum_n j^{\alpha}_{mn}\phi^{\alpha}_{mn},$$

and

$$\hat{E}^{\text{inc}}_\alpha \approx \sum_m \sum_n e^{\text{inc},\alpha}_{mn}\phi^{\alpha}_{mn}.$$

In the first equation $\hat{\mathbf{E}}$, $\hat{\mathbf{E}}^{\text{inc}}$ and $\mathbf{S}(\hat{\mathbf{J}})$ are all expanded in pulse times linear basis functions (rooftop basis functions). In the second equation, $\mathbf{S}(\hat{\mathbf{J}})$ and $\hat{\mathbf{J}}$ are both expanded in pulse times pulse basis functions so that the vector potential is eventually approximated following the midpoint rule. In the third equation, $\hat{\mathbf{J}}$ and $\hat{\mathbf{E}}$ are also both expanded in pulse times pulse basis functions. After applying the weighting procedure to $\hat{\mathbf{J}} = \chi_e\hat{\mathbf{E}}$, the coefficients j^{α}_{mn} can be determined and used to find the coefficients s^{α}_{mn}.

X-COMPONENT

Substitution of the basis functions and the test functions in the weak form for the x-component, gives

$$\begin{aligned}
&\sum_{m=1}^{\mathrm{M}}\sum_{n=1}^{\mathrm{N}} e^x_{mn}\left\{\int_\Omega \Lambda_m(x)\Pi_n(y)\Lambda_p(x)\Pi_q(y)\mathrm{d}\Omega\right\} \quad - \\
&\sum_{m=1}^{\mathrm{M}}\sum_{n=1}^{\mathrm{N}} s^x_{mn}\left\{\int_\Omega \mathrm{k_b^2}\Lambda_m(x)\Pi_n(y)\Lambda_p(x)\Pi_q(y)\mathrm{d}\Omega - \int_\Omega \frac{\partial}{\partial x}\left[\Lambda_m(x)\Pi_n(y)\right]\frac{\partial}{\partial x}\left[\Lambda_p(x)\Pi_q(y)\right]\mathrm{d}\Omega\right\} \quad + \\
&\sum_{m=1}^{\mathrm{M}}\sum_{n=1}^{\mathrm{N}} s^y_{mn}\left\{\int_\Omega \frac{\partial}{\partial y}\left[\Pi_m(x)\Lambda_n(y)\right]\frac{\partial}{\partial x}\left[\Lambda_p(x)\Pi_q(y)\right]\mathrm{d}\Omega\right\} \quad = \\
&\sum_{m=1}^{\mathrm{M}}\sum_{n=1}^{\mathrm{N}} e^{\mathrm{inc},x}_{mn}\left\{\int_\Omega \Lambda_m(x)\Pi_n(y)\Lambda_p(x)\Pi_q(y)\mathrm{d}\Omega\right\} \qquad (3.14)
\end{aligned}$$

for $p = 1,..,\mathrm{M}$ and $q = 1,..,\mathrm{N}$ with M the number of nodes in x-direction and N the number of nodes in y-direction. Each of the integrals can be evaluated making use of the fact that all integrands can be written as a product of functions of x and functions of y.

$$\begin{aligned}
\int_\Omega \Lambda_m(x)\Pi_n(y)\Lambda_p(x)\Pi_q(y)\mathrm{d}\Omega &= \int_x \Lambda_m(x)\Lambda_p(x)\mathrm{d}x\int_y \Pi_n(y)\Pi_q(y)\mathrm{d}y \\
&= \delta_{n,q}\Delta y\int_x \Lambda_m(x)\Lambda_p(x)\mathrm{d}x \\
&= \frac{1}{6}\delta_{n,q}\Delta x\Delta y\left(\delta_{m,p-1}+4\delta_{m,p}+\delta_{m,p+1}\right) \qquad (3.15)
\end{aligned}$$

$$\int_\Omega \mathrm{k_b^2}\Lambda_m(x)\Pi_n(y)\Lambda_p(x)\Pi_q(y)\mathrm{d}\Omega = \frac{1}{6}\mathrm{k_b^2}\delta_{nq}\Delta x\Delta y\left(\delta_{m,p-1}+4\delta_{m,p}+\delta_{m,p+1}\right) \qquad (3.16)$$

$$\begin{aligned}
\int_\Omega \frac{\partial}{\partial y}\left[\Pi_m(x)\Lambda_n(y)\right]\frac{\partial}{\partial x}\left[\Lambda_p(x)\Pi_q(y)\right]\mathrm{d}\Omega &= \int_x\left[\frac{\partial}{\partial x}\Lambda_p(x)\right]\Pi_m(x)\mathrm{d}x\int_y\left[\frac{\partial}{\partial y}\Lambda_n(y)\right]\Pi_q(y)\mathrm{d}y \\
&= -\frac{1}{2}\left(\delta_{m,p+1}-\delta_{m,p-1}\right)\frac{1}{2}\left(\delta_{n,q+1}-\delta_{n,q-1}\right) \qquad (3.17)
\end{aligned}$$

$$\begin{aligned}
\int_\Omega \frac{\partial}{\partial x}\left[\Lambda_m(x)\Pi_n(y)\right]\frac{\partial}{\partial x}\left[\Lambda_p(x)\Pi_q(y)\right]\mathrm{d}\Omega &= \int_x \frac{\partial}{\partial x}\Lambda_m(x)\frac{\partial}{\partial x}\Lambda_p(x)\mathrm{d}x\int_y \Pi_n(y)\Pi_q(y)\mathrm{d}\Omega \\
&= -\delta_{n,q}\frac{1}{\Delta x}\Delta y\left(\delta_{m,p-1}-2\delta_{p,m}+\delta_{m,p+1}\right) \qquad (3.18)
\end{aligned}$$

Substitution of (3.15), (3.16), (3.17) and (3.18) in (3.14) and deviding by $\Delta x\Delta y$ finally gives

$$\begin{aligned}
&\frac{1}{6}\left(e^x_{p-1,q}+4e^x_{p,q}+e^x_{p+1,q}\right)-\frac{1}{6}\mathrm{k_b^2}\left(s^x_{p-1,q}+4s^x_{p,q}+s^x_{p+1,q}\right)-\frac{1}{\Delta x^2}\left(s^x_{p-1,q}-2s^x_{p,q}+s^x_{p+1,q}\right) \\
&-\frac{1}{4\Delta x\Delta y}\left(s^y_{p+1,q+1}-s^y_{p-1,q+1}-s^y_{p+1,q-1}+s^y_{p-1,q-1}\right)=\frac{1}{6}\left(e^{\mathrm{inc},x}_{p-1,q}+4e^{\mathrm{inc},x}_{p,q}+e^{\mathrm{inc},x}_{p+1,q}\right) \qquad (3.19)
\end{aligned}$$

for $p = 1,..,\mathrm{M}$ and $q = 1,..,\mathrm{N}$.

Y-COMPONENT

Substitution of the basis functions and the test functions in the weak form for the $y-$component, gives

$$\sum_{m=1}^{\mathrm{M}}\sum_{n=1}^{\mathrm{N}} e^y_{mn}\left\{\int_\Omega \Pi_m(x)\Lambda_n(y)\Pi_p(x)\Lambda_q(y)\mathrm{d}\Omega\right\} -$$
$$\sum_{m=1}^{\mathrm{M}}\sum_{n=1}^{\mathrm{N}} s^y_{mn}\left\{\int_\Omega \mathrm{k_b^2}\Pi_m(x)\Lambda_n(y)\Pi_p(x)\Lambda_q(y)\mathrm{d}\Omega - \int_\Omega \frac{\partial}{\partial y}\left[\Pi_m(x)\Lambda_n(y)\right]\frac{\partial}{\partial y}\left[\Pi_p(x)\Lambda_q(y)\right]\mathrm{d}\Omega\right\} +$$
$$\sum_{m=1}^{\mathrm{M}}\sum_{n=1}^{\mathrm{N}} s^x_{mn}\left\{\int_\Omega \frac{\partial}{\partial x}\left[\Lambda_m(x)\Pi_n(y)\right]\frac{\partial}{\partial y}\left[\Pi_p(x)\Lambda_q(y)\right]\mathrm{d}\Omega\right\} =$$
$$\sum_{m=1}^{\mathrm{M}}\sum_{n=1}^{\mathrm{N}} e^{\mathrm{inc},y}_{mn}\left\{\int_\Omega \Pi_m(x)\Lambda_n(y)\Pi_p(x)\Lambda_q(y)\mathrm{d}\Omega\right\} \tag{3.20}$$

for $p = 1,..,\mathrm{M}$ and $q = 1,..,\mathrm{N}$ with M the number of nodes in x-direction and N the number of nodes in y-direction. The integrals can be calculated in the same way as for the x-component. The resuts are given by

$$\int_\Omega \Pi_m(x)\Lambda_n(y)\Pi_p(x)\Lambda_q(y)\mathrm{d}\Omega = \frac{1}{6}\delta_{mp}\Delta x\Delta y\left(\delta_{n,q-1}+4\delta_{n,q}+\delta_{n,q+1}\right) \tag{3.21}$$
$$\int_\Omega \mathrm{k_b^2}\Pi_m(x)\Lambda_n(y)\Pi_p(x)\Lambda_q(y)\mathrm{d}\Omega = \frac{1}{6}\mathrm{k_b^2}\delta_{mp}\Delta x\Delta y\left(\delta_{n,q-1}+4\delta_{n,q}+\delta_{n,q+1}\right) \tag{3.22}$$
$$\int_\Omega \frac{\partial}{\partial x}\left[\Lambda_m(x)\Pi_n(y)\right]\frac{\partial}{\partial y}\left[\Pi_p(x)\Lambda_q(y)\right]\mathrm{d}\Omega = -\frac{1}{2}\left(\delta_{m,p+1}-\delta_{m,p-1}\right)\frac{1}{2}\left(\delta_{n,q+1}-\delta_{n,q-1}\right) \tag{3.23}$$
$$\int_\Omega \frac{\partial}{\partial y}\left[\Pi_m(x)\Lambda_n(y)\right]\frac{\partial}{\partial y}\left[\Pi_p(x)\Lambda_q(y)\right]\mathrm{d}\Omega = -\delta_{m,p}\Delta x\frac{1}{\Delta y}\left(\delta_{n,q-1}-2\delta_{n,q}+\delta_{n,q+1}\right). \tag{3.24}$$

Substitution of (3.21), (3.22), (3.23) and (3.24) in (3.20) and deviding by $\Delta x\Delta y$ this time gives

$$\frac{1}{6}\left(e^y_{p,q-1}+4e^y_{p,q}+e^y_{p,q+1}\right)-\frac{1}{6}\mathrm{k_b^2}\left(s^y_{p,q-1}+4s^y_{p,q}+s^y_{p,q+1}\right)-\frac{1}{\Delta y^2}\left(s^y_{p,q-1}-2s^y_{p,q}+s^y_{p,q+1}\right)$$
$$-\frac{1}{4\Delta x\Delta y}\left(s^x_{p+1,q+1}-s^x_{p-1,q+1}-s^x_{p+1,q-1}+s^x_{p-1,q-1}\right)=\frac{1}{6}\left(e^{\mathrm{inc},y}_{p,q-1}+4e^{\mathrm{inc},y}_{p,q}+e^{\mathrm{inc},y}_{p,q+1}\right) \tag{3.25}$$

for $p = 1,..,\mathrm{M}$ and $q = 1,..,\mathrm{N}$.

Now (3.19) and (3.25) can be written as a system like (3.12), but of reduced size because the expressions do not depend on the number of the basis function anymore, only on the number of the test function. In this example the complete system can be calculated quickly by defining central difference matrices. The result would be

$$\begin{aligned} B_\mathrm{N}E^xR_\mathrm{N}^T-\mathrm{k_b^2}B_\mathrm{N}S^xR_\mathrm{N}^T-L_{xx}S^xR_\mathrm{N}^T-L_xS^yL_y &= B_\mathrm{N}E^{\mathrm{inc},x}R_\mathrm{N}^T \\ R_\mathrm{M}E^yB_\mathrm{M}^T-\mathrm{k_b^2}R_\mathrm{M}S^yB_\mathrm{M}^T-R_\mathrm{M}S^yL_{yy}^T-L_xS^xL_y &= R_\mathrm{M}E^{\mathrm{inc},y}B_\mathrm{M}^T \end{aligned}$$

where

$$B_\mathrm{M}^{(\mathrm{M}\times\mathrm{M}+2)}=\frac{1}{6}\begin{bmatrix}1&4&1&&&\\&\ddots&\ddots&\ddots&0&\\&0&\ddots&\ddots&\ddots&\\&&&1&4&1\end{bmatrix}\quad\text{and}\quad B_\mathrm{N}^{(\mathrm{N}\times\mathrm{N}+2)}=\frac{1}{6}\begin{bmatrix}1&4&1&&&\\&\ddots&\ddots&\ddots&0&\\&0&\ddots&\ddots&\ddots&\\&&&1&4&1\end{bmatrix}.$$

The finite difference matrices are written as

$$L_{xx}^{(\mathrm{M}\times\mathrm{M}+2)}=\frac{1}{\Delta x^2}\begin{bmatrix}1&-2&1&&&\\&\ddots&\ddots&\ddots&0&\\&0&\ddots&\ddots&\ddots&\\&&&1&-2&1\end{bmatrix}\quad\text{and}\quad L_{yy}^{(\mathrm{N}\times\mathrm{N}+2)}=\frac{1}{\Delta y^2}\begin{bmatrix}1&-2&1&&&\\&\ddots&\ddots&\ddots&0&\\&0&\ddots&\ddots&\ddots&\\&&&1&-2&1\end{bmatrix},$$

$$L_x^{(\mathrm{M}\times\mathrm{M}+2)} = \frac{1}{2\Delta x}\begin{bmatrix} -1 & 0 & 1 & & & \\ & \ddots & \ddots & \ddots & 0 & \\ & 0 & \ddots & \ddots & \ddots & \\ & & & -1 & 0 & 1 \end{bmatrix} \quad \text{and} \quad L_y^{(\mathrm{N}\times\mathrm{N}+2)} = \frac{1}{2\Delta y}\begin{bmatrix} -1 & 0 & 1 & & & \\ & \ddots & \ddots & \ddots & 0 & \\ & 0 & \ddots & \ddots & \ddots & \\ & & & -1 & 0 & 1 \end{bmatrix}.$$

Finally, the matrices

$$R_{\mathrm{M}}^{(\mathrm{M}\times\mathrm{M}+2)} = \begin{bmatrix} 0 & 1 & & & & 0 \\ \vdots & & \ddots & 0 & & \vdots \\ \vdots & & 0 & \ddots & & \vdots \\ 0 & & & & 1 & 0 \end{bmatrix} \quad \text{and} \quad R_{\mathrm{N}}^{(\mathrm{N}\times\mathrm{N}+2)} = \begin{bmatrix} 0 & 1 & & & & 0 \\ \vdots & & \ddots & 0 & & \vdots \\ \vdots & & 0 & \ddots & & \vdots \\ 0 & & & & 1 & 0 \end{bmatrix}$$

strip the first and the last row or column of matrices respectively.

The matrices S^x and S^y are constructed in a couple of steps. First note that

$$\begin{aligned} S(\hat{J}_\alpha)(\mathbf{x}) &= \int_{\mathbf{x}'} \hat{g}(\mathbf{x}-\mathbf{x}')\hat{J}_\alpha(\mathbf{x}')\mathrm{d}\mathbf{x}' \\ &= \int_{\mathbf{x}'} \hat{g}(\mathbf{x}-\mathbf{x}') \sum_{m=1}^{\mathrm{M}}\sum_{n=1}^{\mathrm{N}} j_{mn}\Pi_m(x')\Pi_n(y')\mathrm{d}\mathbf{x}' \\ &= \sum_{m=1}^{\mathrm{M}}\sum_{n=1}^{\mathrm{N}} j_{mn}\hat{g}(\mathbf{x}-\mathbf{x}_{mn})\Delta x\Delta y \end{aligned}$$

and

$$\begin{aligned} \int_\Omega \sum_k\sum_l s_{kl}\Pi_k(x)\Pi_l(y)\Pi_p(x)\Pi_q(y)d\Omega &= \int_\Omega \sum_m\sum_n j^\alpha_{mn}\hat{g}(\mathbf{x}-\mathbf{x}_{mn})\Delta x\Delta y\Pi_p(x)\Pi_q(y)\mathrm{d}\Omega \Leftrightarrow \\ \sum_k\sum_l s_{kl}\delta_{kp}\delta_{lq}\Delta x\Delta y &= \sum_m\sum_n j^\alpha_{mn}\Delta x\Delta y\int_\Omega \hat{g}(\mathbf{x}-\mathbf{x}_{mn})\Pi_p(x)\Pi_q(y)\mathrm{d}\Omega \Rightarrow \\ s_{pq} &\approx \sum_m\sum_n j^\alpha_{mn}\hat{g}(\mathbf{x}_{pq}-\mathbf{x}_{mn})\Delta x\Delta y. \end{aligned} \tag{3.26}$$

Furthermore, the weighting procedure applied to $\hat{\mathbf{J}} = \chi_{\mathrm{e}}\hat{\mathbf{E}}$ determines the coefficients j^α_{mn}. It follows that

$$\begin{aligned} \int_\Omega \sum_m\sum_n j^\alpha_{mn}\Pi_m(x)\Pi_n(y)\Pi_p(x)\Pi_q(y)\mathrm{d}\Omega &= \int_\Omega \chi_{\mathrm{e}}\sum_m\sum_n e^\alpha_{mn}\Pi_m(x)\Pi_n(y)\Pi_p(x)\Pi_q(y)\mathrm{d}\Omega \Leftrightarrow \\ j^\alpha_{pq}\Delta x\Delta y &= \sum_m\sum_n e^\alpha_{mn}\int_\Omega \chi_{\mathrm{e}}\Pi_m(x)\Pi_n(y)\Pi_p(x)\Pi_q(y)\mathrm{d}\Omega \Rightarrow \\ j^\alpha_{pq} &\approx \chi_{\mathrm{e}_{pq}}e^\alpha_{pq} \end{aligned} \tag{3.27}$$

where in the last step the contrast function is assumed to be constant within each voxel.

Substituting (3.27) in (3.26) gives the final expression for the coefficients of the matrices S^x and S^y. The first possibility is to compute each coefficient seperately by evaluating (3.26) for each node p, q. The second possibility is to recognise a convolution in (3.26) and compute the result with fast fourier transforms (FFT). In practise the second possibility will always be used when possible, because it reduces the computation time considerably.

3.6. RESULTS

The methods discussed in 3.4 and 3.5 have both been tested with 61 grid nodes in each direction. In the test case the incident field, a plane wave, enters a rectangular region. The incident field points in the x-direction and propagates in the y-direction, described as $E_x(x,y) = e^{-\mathrm{i}k_{\mathrm{b}}y}$ and $E_y(x,y) = 0$. In the middle of the rectangular region there is a circular region with a permittivity of five times the background permittivity. The diameter of the circle is 0.14 meters and the background material has the permittivity of vacuum. There is no conduction in this case and the frequency used is $128\cdot 10^6$ Hz. Figures 3.4a and 3.4b show the absolute value

of the x-component and the y-component of the resulting electric field obtained with the method described in Example 1. Figures 3.6a and 3.6b show the x-component and the y-component of the resulting electric field obtained with the method described in Example 2. As can be seen in those figures, the circular region scatters the plane wave in x- and y-directions. In all figures ten percent of the domain has been cut off from all boundaries. This is done because at this point the method described in Example 1 shows inaccuracies at the boundaries.
Figures 3.5 and 3.7 show the behaviour of the electric fields along the symmetry axes of the circular domain. Example 2 has also been tested with a finer mesh and it resulted in a better accuracy. An important point of focus is that the tangential components of the electric field (E_y along x and E_x along y) have to be continuous as the boundary conditions prescribe, and the normal components (E_y along y and E_x along x) may be discontinuous. Figure 3.8 shows the electric fields along the axes for the case where tested with 257 grid nodes in each direction. Example 1 has not been tested with the same resolution because of memory limitations.

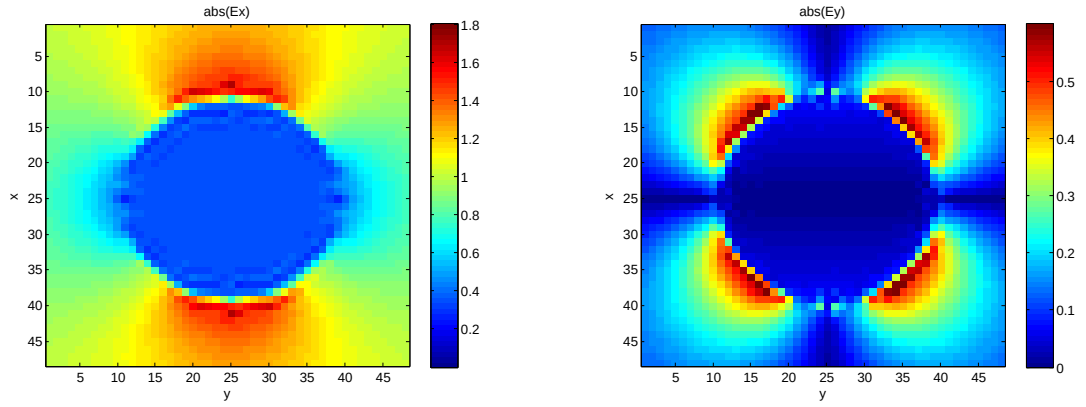

(a) (b)

Figure 3.4: Absolute value of the electric fields in x- and y-directions obtained with the method explained in Example 1 and 61 grid nodes per direction.

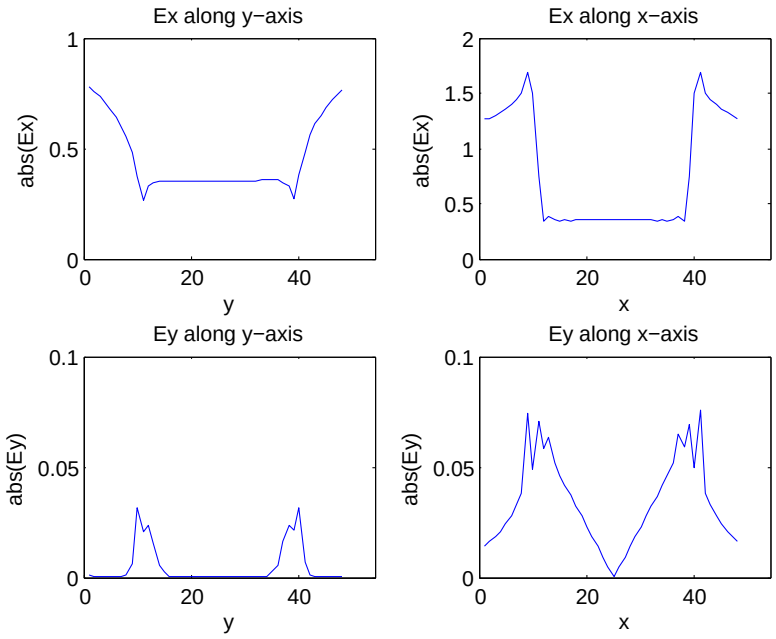

Figure 3.5: Electric fields along the axes obtained with the method explained in Example 1 and 61 grid nodes per direction.

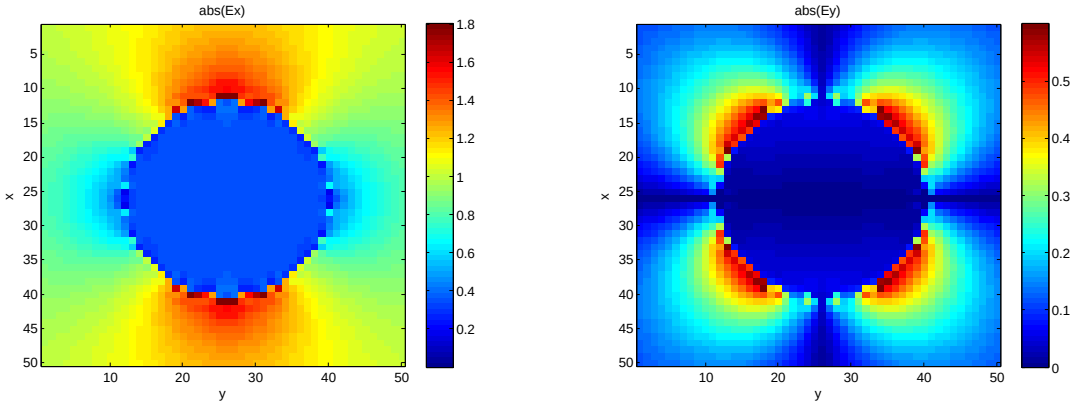

(a) (b)

Figure 3.6: Electric fields in x- and y-directions obtained with the method explained in Example 2 and 61 grid nodes per direction.

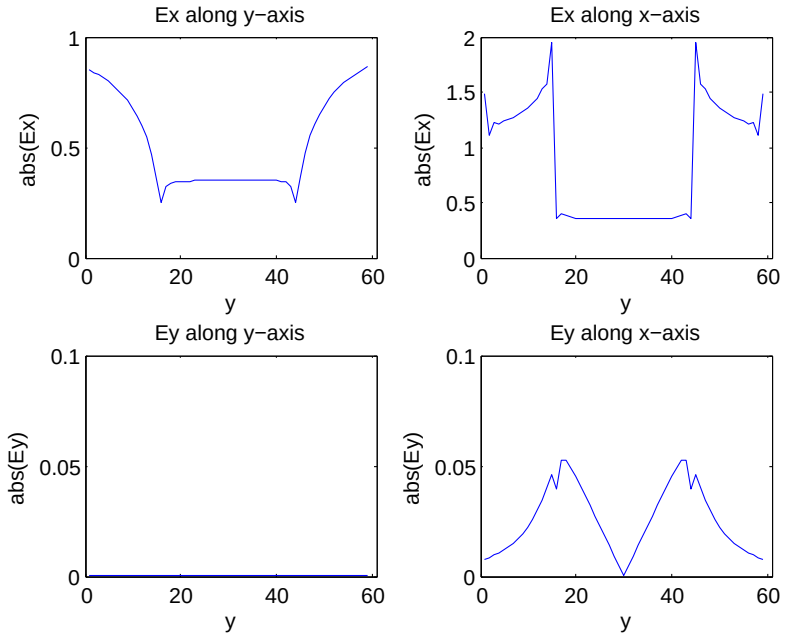

Figure 3.7: Electric fields along the axes obtained with the method explained in Example 2 and 61 grid nodes per direction.

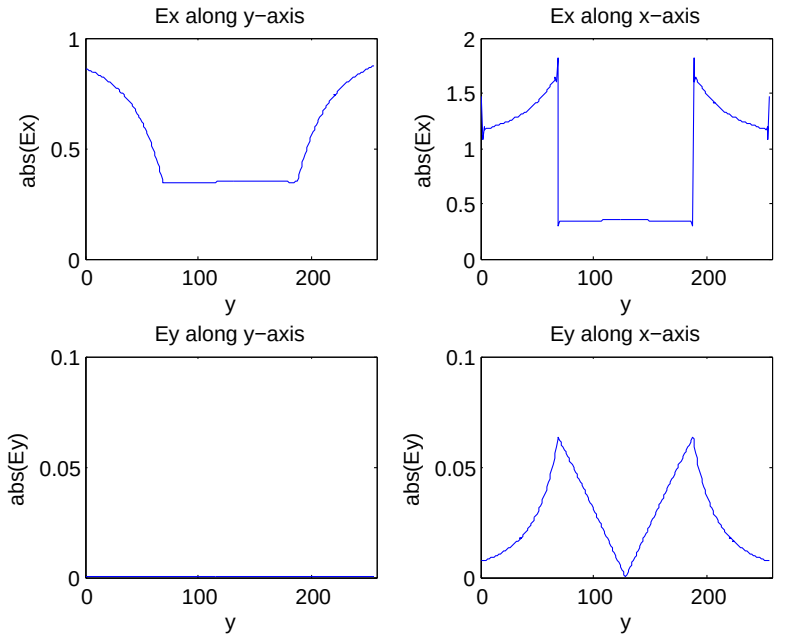

Figure 3.8: Electric fields along the axes obtained with the method explained in Example 2 and 257 grid nodes per direction.

4

SOLVERS

Once a discretised system $A\mathbf{x} = \mathbf{b}$ has been obtained, it can be solved with several numerical solution methods. Which ones are suitable depends among others on the structure of the system matrix and the problem size. Smaller systems are usually solved with a direct solution methods like *LU* decomposition or Cholesky decomposition. For larger systems one should switch to iterative solution methods. Also in the method explained in Section 3.5 an iterative solution method is preferable, because then matrix vector products can be accelerated by using fast fourier transforms.
Two groups of iterative methods are Basic Iterative Methods (BIM's) and Krylov Subspace Methods. Basic Iterative Methods form the basis of the more advanced Krylov Subspace Methods. In this chapter some of the Krylov Subspace Methods will be discussed.

Krylov subspace methods are based on the idea that the iterated solution $\mathbf{x}^i$ is an element of $\mathscr{K}^i(A;\mathbf{r}^0)$, where

$$\mathscr{K}^i(A;\mathbf{r}^0) = \text{span}\left\{\mathbf{r}^0, A\mathbf{r}^0, ..., A^{i-1}\mathbf{r}^0\right\} \tag{4.1}$$

For systems with a symmetric positive definite system matrix A, the Chebyshev method and Conjugent Gradient (CG) method can be used. However, for scattering problems the system matrix is in general not symmetric. Also for these matrices Krylov Subspace Methods have been developed. Bi-CG, Bi-CGSTAB, GMRES and IDR(s) are methods of this kind. In this chapter GMRES and IDR(s) will be discussed briefly.

4.1. GMRES

In each iteration of the GMRES method the solution is approximated such that

$$||\mathbf{r}^i||_2 = ||\mathbf{b} - A\mathbf{x}^i||_2 = \min_{\mathbf{z}\in\mathscr{K}^i(A,\mathbf{r}^0)}||\mathbf{r}^0 - A\mathbf{z}||_2. \tag{4.2}$$

This means that the residual in iteration i is orthogonal to $A\mathscr{K}^i(\mathbf{A};\mathbf{r}^0)$. GMRES is a stable method with superlinear convergence in many cases. However, GMRES is also an example of a method with long recurrences, which means that the work per iteration and memory requirements increase as the number of iterations increases. A solution to this problem is to restart GMRES after a certain number of iterations with the last approximate solution as a starting vector. Drawbacks of this approach are that optimality and superlinear convergence are lost.

4.2. IDR(s)

The Induced Dimension Reduction method (IDR(s)) is a relatively new method that is used to solve large nonsymmetric systems. The idea behind the method is based on the IDR theorem of which a generalised version has been published in [5]:

Theorem 2. *Let A be any matrix in $\mathbb{C}^{N\times N}$, let $\mathbf{v}_0$ be any nonzero vector in $\mathbb{C}^N$, and let $\mathscr{G}_0$ be the full Krylov space $\mathscr{K}^N(A,\mathbf{v}_0)$. Let $\mathscr{S}$ denote any (proper) subspace of $\mathbb{C}^N$ such that $\mathscr{S}$ and $\mathscr{G}_0$ do not share a nontrivial invariant subspace of A, and define the sequence $\mathscr{G}_j$, $j = 1,2,...,$ as*

$$\mathscr{G}_j = (I - \omega_j A)(\mathscr{G}_{j-1} \cap \mathscr{S}),$$

where the ω_j's are nonzero scalars. Then the following hold:
i) $\mathcal{G}_j \subset \mathcal{G}_{j-1} \forall\, j > 0$.
ii) $\mathcal{G}_j = \{\mathbf{0}\}$ *for some* $j \leq N$.

In the algorithm the residuals $\mathbf{r}^i$ are forced to be elements of the nested subspaces $\mathcal{G}_i$. These subspaces are decrasing in dimension, which means that there is a residual $\mathbf{r}_m$ that is an element of $\mathcal{G}_m = \{\mathbf{0}\}$. Once this residual is obtained, the algorithm stops.

4.3. PRECONDITIONING

In order to accelerate convergence, both sides of the equation $A\mathbf{x} = \mathbf{b}$ can be multiplied with a preconditioner M. By doing this, a new system with system matrix $M^{-1}A$ arises. By choosing the precondioner wisely, the spectrum of the new system matrix can become much more favorable (clustered around 1) which in turn results in faster convergence. Ideally the matrix M would be equal to A, but the computation of A^{-1} is very expensive for systems that are being solved iteratively. A preconditioner equal to the identity matrix would result in a fast computation of $M^{-1}A$, but then the spectrum of the system matrix does not improve. In practice the preconditioner is chosen somewhere in between.

5

NUMERICAL CHALLENGES

There are a couple of numerical challenges that have to be dealt with. In this chapter those numerical challenges will be described and clearified with figures.

In Chapter 1 it has already been discussed that the method described in Section 3.5 shows inaccuracies at permittivity interfaces. This inaccuracy is visible only in case of a lossy dielectric material, which means that there is conduction. To show the inacurracy, the electric field is approximated when scattering on a two-layered cylinder. The outer layer has a relative permittivity of 7.5 and a conductivity of 0.048 siemens per meter. The inner cylinder has a relative permittivity of 72 and a conductivity of 0.9 siemens per meter. The cylinder is surrounded by vacuum and the incident field points in the x-direction and propagates in the y-direction.
Figure 5.1 shows the electric field along the symmetry axes of the cylinders in this situation. The electric jumps are clearly visible in the graph for the y-component of the electric field along the x-axis and slightly less visible in the graph for the x-component along the y-axis. These components correspond with the tangential components of the electric field along the cylinder layers. The boundary conditions of Maxwell's equations, however, tell that these components are supposed to be continuous.
The jumps occur at permittivity interfaces only. This gives rise to the idea that weakening the contrast function at permittivity interfaces would improve the results. Weakening the contrast function can be seen as a result of choosing different basis functions. Using an expansion with linear basis functions in both x- and y-directions indeed decreases the jumps, as can be seen in Figure 5.2. Even though in this case the contrast function is weakened by averaging over the four neighbouring grid points, a jump is still there. Moreover, when working with lower resolution, the improved result is even more different from what is expected.

The second thing that attracts attention is that in the method described in Section 3.4, the electric field blows up at the boundaries of the compuational domain. Also in the method described in Section 3.5 a jump is visible at the boundary, although much smaller than in Section 3.4. At this point it is not clear what is causing this.

One general requirement that has to be taken into account is that the computation time has to be kept short. The triangular mesh with grid points at the vertices of the triangle results in a long computation time because the system matrix is being filled via assembly. The rectangular mesh with grid points at the centers of the voxels results in a shorter computation time, because the entire system matrix can be constructed via matrix vector products.

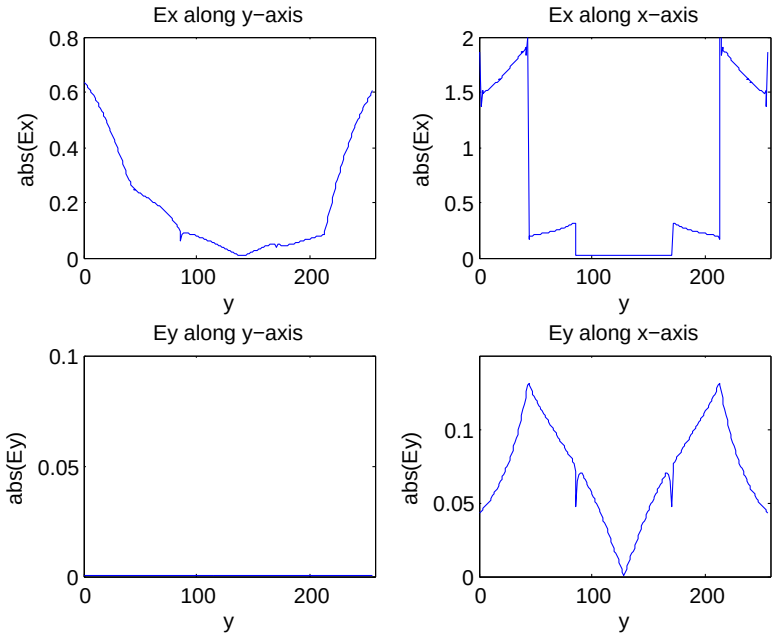

Figure 5.1: Electric fields along the axes obtained with the method explained in Example 2 and 257 grid nodes per direction.

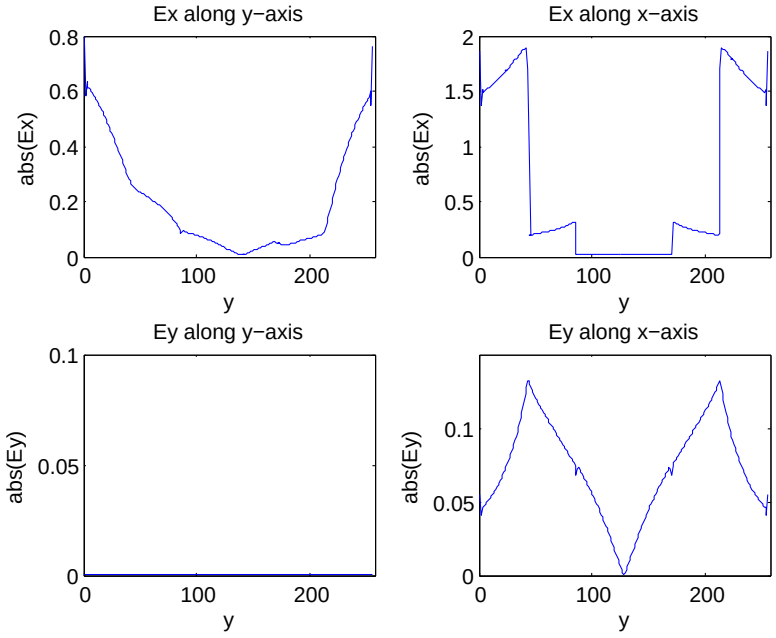

Figure 5.2: Electric fields along the axes obtained with the method explained in Example 2 and 257 grid nodes per direction.

6

GOAL OF THE PROJECT AND WORKING METHOD

As described in Chapter 5 a couple of problems have to be dealt with. In this chapter some ideas will be proposed that could result in a better solution method. The main goals are

1. to obtain an accurate solution and
2. to obtain it fast.

From studying the literature, two things come forward. The first observation is that the choice of basis functions affects the results considerably. This was also shown in Chapter 5. Second, different formulations result in different accuracies, see [6]. Warnings regarding convergence have been made in [7]: choose the right basis functions for a specific formulation. The choice of basis functions seems to be very closely related to the choice of formulation. Finally, the mesh is a variable aspect as well.

6.1. PROBLEM FORMULATION

In order to continue the research, two things have to be decided. What kind of mesh will be chosen and which formulation will be implemented?
Earlier it was discussed that a triangular mesh with grid points at the vertices implies a long computation time because of matrix assembly. The conventional method is to choose a rectangular mesh with grid points at the centers, like in the method in Section 3.5. Also this study will focus on the rectangular mesh.
In order to choose a formulation, it is interesting to have a look what has been done already. Several people have been working with the rectangular mesh and Table 6.1 gives a short summary of the methods used. In [8] and [9] P. Zwamborn tests his method on the two-layered cylinder and does not find any surprising jumps. In contrast to the method described in Section 3.4, P. Zwamborn weakens the constrast function before he applies the testing procedure. Also the formulation is different: P. Zwamborn chooses for the DVIE formulation instead of the EVIE formulation. Therefore the question arises how well the method in Section 3.5 performs, once formulated in term of the displacement current.
There is one general fact that has to be taken into account when choosing a formulation and basis functions. For Galerkin's Method to converge in norm, the test functions should span the dual space of the range of the operator corresponding with the volume integral equation. Many methods do not take this into account. The range of the EVIE formulation contains all functions that are square integrable and who's divergence is square integrable as well. The dual range is therefore a larger function space than $[L^2(\mathbb{R}^3)]^3$ and it is not straightforward how to choose test functions that span this space. The same holds for the DVIE formulation.
A possibility is to avoid this problem is to use the JVIE formulation. The range of the JVIE operator is $[L^2(\mathbb{R}^3)]^3$ and its dual is again $[L^2(\mathbb{R}^3)]^3$. Therefore the basis and test functions can be chosen such that they span the function space $[L^2(\mathbb{R}^3)]^3$. Functions that span $[L^2(\mathbb{R}^3)]^3$ are for example step functions, but also rooftop functions or linear functions in all directions. Again it is important to take into account the behaviour of $\mathbf{J}$ when choosing the test functions. From the $\mathbf{E}$ and $\mathbf{D}$ boundary conditions and the expression for $\mathbf{J}$ one can derive that the normal and the tangential components of the induced current density should be discontinuous. This

means that in the JVIE formulation constant basis functions in both directions would take into account the physical properties of **J** better than rooftop basis functions.

Name	Weak Form	Formulation	Expansion	Mesh	Basis functions	Grid points
Abubakar	1	EVIE	$\mathbf{E}, \mathbf{S}, \mathbf{E}^{\text{inc}}$	Voxel	Rooftop	Middle
Kooij	1	EVIE	$\mathbf{E}$	Voxel	Rooftop	Middle
Polimeridis	2	JVIE	$\mathbf{J}, \varepsilon$	Voxel	Pulse	Middle
Stijlen	1	EVIE	$\mathbf{E}, \mathbf{S}, \mathbf{E}^{\text{inc}}$	Voxel	Rooftop	Middle
Zwamborn	2	DVIE	$\mathbf{D}, \mathbf{S}, \mathbf{E}^{\text{inc}}$	Voxel	Rooftop	Middle
Zwamborn	2	DVIE	$\mathbf{D}, \mathbf{S}$	Voxel	Rooftop	Staggered, at boundaries

Table 6.1: Overview of previous methods.

6.2. APPROACH

The first part of the research will focus on the accuracy of the solution and in particular on localising the cause of the jumps that were shown in Chapter 5. Since two methods are available, one that works (P. Zwamborn) and one that does not work accurately (described in Section 3.5), it is interesting to compare the two methods. In order to find the step that causes the problem, the following poceedings will be carried out.

- Expanding **J** in Section 3.5 with linear basis functions so that all expansions are consequent.
- Implement the DVIE formulation with rooftop basis functions to check the method in Section 3.5 with Zwamborn's method.
- If the latter step makes no or insufficient difference, the contrast function will be weakened before the expansion procedure takes place.
- Implement the JVIE formulation with rooftop basis functions to see the difference between the EVIE, DVIE and JVIE formulations.
- Run the triangle example with linear basis functions on a server to check whether jump is visible in this case. This method differs from the conventional method on the following aspects: grid points at the vertices of elements, linear basis functions in all directions and a triangular mesh.
- Check whether the jumps are caused by inaccurate modeling of the borders of high permittivity domains by choosing clever geometries.

Once an accurate solution has been obtained, the aim is to reduce the computation time by applying a suitable iterative method. First GMRES will be applied and later IDR(s) will be studied as a new alternative iterative method.

6.3. BENCHMARK PROBLEM

To study the performance of future methods, a benchmark problem is introduced. The transverse electric (TE) polarisation is considered, which means that the electric field has its components in the transverse (xy-) plane and the magnetic field is perpendicular to the electric field. This means that a $2D$ configuration is satisfactory to model the electric field.
The $2D$ benchmark problem consists of a rectangular region with a two-layered cylinder in the middle. The outer layer has a relative permittivity of 7.5 and a conductivity of 0.048 siemens per meter. The inner cylinder has a relative permittivity of 72 and a conductivity of 0.9 siemens per meter. The cylinder is surrounded by vacuum and the incident field points in the x-direction and propagates in the y-direction. Figure 6.1a schematically shows the situation. In this figure $\varepsilon_r = \frac{\varepsilon}{\varepsilon_0}$.
Next to this benchmark problem, also the configuration shown in Figure 6.1b will be studied. Earlier studies showed that in this case, where one of the directional derivatives is zero, no jump is visible. In order to exclude the staircasing effect from the list of causes for the jumps, the incident field can be changed from a plane wave propagating in one direction to a plane wave propagating in two directions. By doing this, the borders of the domain with high permittivity are modeled accurately and both directional derivatives exist.

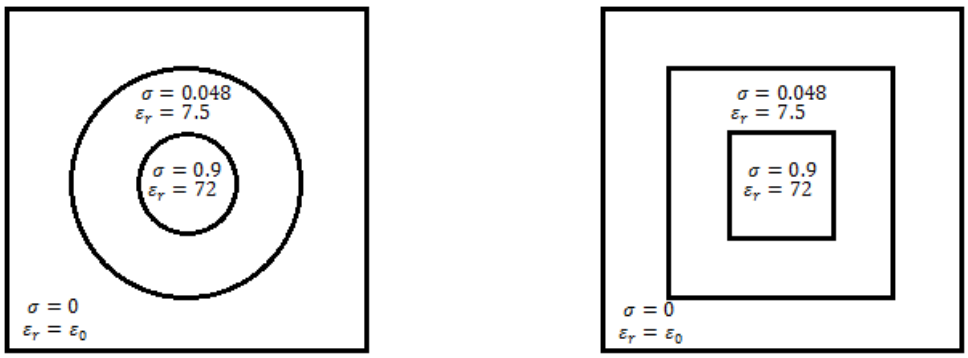

(a) (b)

Figure 6.1: Benchmark problems with different geometries.

A

Inverse Fourier Transform of the Green's Function

First the identity

$$\gamma_0 = \sqrt{\eta_0 \xi_0} = \sqrt{(s\varepsilon_0)(s\mu_0)} = s\sqrt{\varepsilon_0\mu_0} = \frac{s}{c} = \frac{s}{\omega}\mathrm{k_b} \overset{s=\omega \mathrm{i}}{=} \mathrm{k_b i}$$

is introduced. The Green's function therefore translates to

$$\tilde{g} = \frac{1}{\mathbf{k}^T\mathbf{k} - \mathrm{k_b^2}}$$

and in two dimensions,

$$\begin{aligned}
\hat{g}(\mathbf{x}, s) &= \frac{1}{(2\pi)^2}\int_{\mathbf{k}\in\mathbb{R}^2} \frac{1}{\mathbf{k}^T\mathbf{k} - \mathrm{k_b^2}} e^{-\mathrm{i}\mathbf{k}\cdot\mathbf{x}} \mathrm{d}V \\
&= \frac{1}{(2\pi)^2}\int_{\mathbf{k}\in\mathbb{R}^2} \frac{1}{k_1^2 + k_2^2 - \mathrm{k_b^2}} e^{-\mathrm{i}k_1x_1 - \mathrm{i}k_2x_2} \mathrm{d}V \\
&\overset{\Gamma=\sqrt{\mathrm{k_b^2}-k_1^2}}{=} \frac{1}{(2\pi)^2}\int_{k_1\in\mathbb{R}} e^{-\mathrm{i}k_1x_1}\int_{k_2\in\mathbb{R}} \frac{1}{k_2^2 - \Gamma^2} e^{-\mathrm{i}k_2x_2}\mathrm{d}k_2\mathrm{d}k_1.
\end{aligned}$$

Since the function in the inner integral has two simple poles, the residue theorem gives

$$\int_C \frac{1}{z^2-\Gamma^2} e^{-\mathrm{i}zx_2}\mathrm{d}z = 2\pi\mathrm{i}\,\mathrm{Res}(f,\Gamma) = \frac{\pi\mathrm{i}}{\Gamma}e^{-\mathrm{i}\Gamma|x_2|},$$

where C is the closed curve along the semicircle with radius R in the upper half plane and $f(z) = \frac{1}{z^2-\Gamma^2}e^{-\mathrm{i}zx_2}$. The integral along the curved path $\beta_r = Re^{\mathrm{i}t}$ drops to zero when $R\to\infty$, since

$$\left|\int_{\beta_r} \frac{1}{z^2-\Gamma^2} e^{-\mathrm{i}zx_2}\mathrm{d}z\right| = \left|\int_{\beta_r} \frac{R\mathrm{i}}{+R^2e^{2\mathrm{i}t} - \Gamma^2} e^{\mathrm{i}(t - Re^{\mathrm{i}t}x_2)}\mathrm{d}t\right| \le \int_{\beta_r} \frac{|R\mathrm{i}|}{\left|R^2e^{2\mathrm{i}t} - \Gamma^2\right|}\left|e^{\mathrm{i}(t-Re^{\mathrm{i}t}x_2)}\right| dt \le \int_{\beta_r} \frac{1}{\left|Re^{2\mathrm{i}t} - \frac{\Gamma^2}{R}\right|}\mathrm{d}t.$$

Therefore

$$\int_{k_2\in\mathbb{R}} \frac{1}{k_2^2-\Gamma^2} e^{-\mathrm{i}k_2x_2}\mathrm{d}k_2 = \frac{\pi\mathrm{i}}{\Gamma}e^{-\mathrm{i}\Gamma|x_2|}$$

and

$$\begin{aligned}
\hat{g}(\mathbf{x}, s) &= \frac{\mathrm{i}}{4\pi}\int_{k_1\in\mathbb{R}} \frac{e^{-\mathrm{i}k_1x_1 - \mathrm{i}\Gamma|x_2|}}{\Gamma}\mathrm{d}k_1 \\
&= \frac{\mathrm{i}}{4\pi}\int_{k_1\in\mathbb{R}} \frac{e^{-\mathrm{i}k_1x_1 + \sqrt{k_b^2-k_1^2}|x_2|}}{\sqrt{\mathrm{k_b^2} - k_1^2}}\mathrm{d}k_1.
\end{aligned} \tag{A.1}$$

In (A.1) a Hankelfunction of the second kind can be recognised. [10] states

$$\hat{g}(\mathbf{x}, s) = -\frac{\mathrm{i}}{4}H_0^{(2)}(\mathrm{k_b}|x|).$$

B

Weakening of the Green's Function

The function

$$\hat{g}(\mathbf{x}, s) = -\frac{\mathrm{i}}{4} H_0^{(2)}(\mathrm{k_b}|\mathbf{x}|)$$

has a singularity at $\mathbf{x} = 0$.

Recall that the Green's function satisfies

$$\nabla^2 \hat{g}(\mathbf{x}, s) + \mathrm{k_b}^2 \hat{g}(\mathbf{x}, s) = -\delta(\mathbf{x}).$$

In order to avoid the singularity in the Green's function, the whole function is approximated by a 'weakened' Green's function, that satisfies

$$\nabla^2 \hat{g}^{\mathrm{w}}(\mathbf{x}, s) + \mathrm{k_b}^2 \hat{g}^{\mathrm{w}}(\mathbf{x}, s) = -f(\mathbf{x}) \tag{B.1}$$

with

$$f(\mathbf{x}) = \begin{cases} \frac{1}{\pi a^2} & \text{if } \mathbf{x} \in \mathbb{D} \\ 0 & \text{if } \mathbf{x} \notin \mathbb{D} \end{cases}$$

and $\mathbb{D}$ a circular domain with radius $\mathrm{a} = \frac{1}{2}\min\{\Delta x \Delta y\}$. In this way $\mathbb{D}$ is contained in one cell and the function $f(\mathbf{x})$ approaches the Dirac delta function as $\mathrm{a} \downarrow 0$.

The solution of (B.1) is given by

$$\begin{aligned} \hat{g}^{\mathrm{w}}(\mathbf{x}, s) &= \int_{\mathbf{x}' \in \mathbb{R}^2} \hat{g}(\mathbf{x} - \mathbf{x}', s) f(\mathbf{x}') \mathrm{d}V' \\ &= \frac{1}{\pi \mathrm{a}^2} \int_{\mathbf{x}' \in \mathbb{D}} \hat{g}(\mathbf{x} - \mathbf{x}', s) \mathrm{d}V' \end{aligned}$$

In order to actually compute $\hat{g}^{w}$ the problem is split in two cases: $\mathbf{x} \notin \mathbb{D}$ and $\mathbf{x} \in \mathbb{D}$. In both cases the integral

$$\hat{g}^{\mathrm{w}}(\mathbf{x}, s) = -\frac{i}{4\pi \mathrm{a}^2} \int_{\mathbf{x}' \in \mathbb{D}} H_0^{(2)}(\mathrm{k_b}|\mathbf{x} - \mathbf{x}'|) \mathrm{d}V' \tag{B.2}$$

has to be evaluated.

The Hankel function inside the integral can be written as an infinite sum, using the addition theorem for the Hankel function $H_0^{(2)}$ which can be found in [11]. With ϕ the angle between $\mathbf{x}$ and $\mathbf{x}'$ and J_k the k-th order Bessel function of the first kind, the result is given by

$$H_0^{(2)}(\mathrm{k_b}|\mathbf{x} - \mathbf{x}'|) = \begin{cases} \sum_{k=-\infty}^{\infty} J_k(\mathrm{k_b}|\mathbf{x}|) H_k^{(2)}(\mathrm{k_b}|\mathbf{x}'|) e^{\mathrm{i}k\phi}, & |\mathbf{x}| \leq |\mathbf{x}'| \\ \sum_{k=-\infty}^{\infty} J_k(\mathrm{k_b}|\mathbf{x}'|) H_k^{(2)}(\mathrm{k_b}|\mathbf{x}|) e^{\mathrm{i}k\phi}, & |\mathbf{x}'| \leq |\mathbf{x}| \end{cases}. \tag{B.3}$$

In the first case, where $\mathbf{x} \notin \mathbb{D}$, it holds that $|\mathbf{x}| > |\mathbf{x}'|$ for all $\mathbf{x}' \in \mathbb{D}$ and therefore

$$\hat{g}^{\mathrm{w}}(\mathbf{x}, s) = -\frac{\mathrm{i}}{4\pi \mathrm{a}^2} \int_{\mathbf{x}' \in \mathbb{D}} \sum_{k=-\infty}^{\infty} J_k(\mathrm{k_b}|\mathbf{x}'|) H_k^{(2)}(\mathrm{k_b}|\mathbf{x}|) e^{\mathrm{i}k\phi} \mathrm{d}V'. \tag{B.4}$$

Transforming (B.4) into polar coordinates, gives

$$\begin{aligned}
\hat{g}^{\mathrm{w}}(\mathbf{x},s) &= -\frac{\mathrm{i}}{4\pi \mathrm{a}^2}\int_0^{2\pi}\int_0^{\mathrm{a}}\sum_{k=-\infty}^{\infty} J_k(k_b r)H_k^{(2)}(k_b|\mathbf{x}|)e^{ik\phi}r\,\mathrm{d}r\,\mathrm{d}\phi \\
&= -\sum_{k=-\infty}^{\infty}\frac{\mathrm{i}}{4\pi \mathrm{a}^2}H_k^{(2)}(\mathrm{k_b}|\mathbf{x}|)\int_0^{2\pi}e^{\mathrm{i}k\phi}\mathrm{d}\phi\int_0^{\mathrm{a}}J_k(\mathrm{k_b}r)r\,\mathrm{d}r \\
&= -\frac{\mathrm{i}}{2\mathrm{a}^2}H_0^{(2)}(\mathrm{k_b}|\mathbf{x}|)\int_0^{\mathrm{a}}J_0(\mathrm{k_b}r)r\,\mathrm{d}r \\
&= -\frac{\mathrm{i}}{2\mathrm{a}^2}H_0^{(2)}(\mathrm{k_b}|\mathbf{x}|)\frac{1}{\mathrm{k_b}^2}\int_0^{\mathrm{k_b a}}zJ_0(z)\mathrm{d}z \\
&= -\frac{\mathrm{i}}{2\mathrm{a}^2}H_0^{(2)}(\mathrm{k_b}|\mathbf{x}|)\frac{1}{\mathrm{k_b}^2}\int_0^{\mathrm{k_b a}}\frac{\mathrm{d}}{\mathrm{d}z}\left(zJ_1(z)\right)dz \\
&= -\frac{i}{2\mathrm{ak_b}}H_0^{(2)}(\mathrm{k_b}|\mathbf{x}|)J_1(\mathrm{k_b a}).
\end{aligned}$$

In the second case, where $\mathbf{x}\in\mathbb{D}$, only $\hat{g}^{\mathrm{w}}(\mathbf{0},s)$ is of interest for the discretisation procedure. To obtain this value, $|\mathbf{x}|=\varepsilon<a$ is fixed after which the limit $\varepsilon\downarrow 0$ is taken. The integration region is split in two parts: the circular disc $\mathbb{D}_\varepsilon$ with radius ε and the rest of $\mathbb{D}$, denoted by $\mathbb{D}\setminus\mathbb{D}_\varepsilon$. In the point $\mathbf{x}=\mathbf{0}$ (B.2) now becomes

$$\hat{g}^{w}(\mathbf{0},s) = -\frac{\mathrm{i}}{4\pi \mathrm{a}^2}\lim_{\varepsilon\downarrow 0}\left[\int_{\mathbf{x}'\in\mathbb{D}_\varepsilon}H_0^{(2)}(\mathrm{k_b}|\mathbf{x}-\mathbf{x}'|)\mathrm{d}V'+\int_{\mathbf{x}'\in\mathbb{D}\setminus\mathbb{D}_\varepsilon}H_0^{(2)}(\mathrm{k_b}|\mathbf{x}-\mathbf{x}'|)\mathrm{d}V'\right]. \tag{B.5}$$

For the second integral in (B.5) it holds that $|\mathbf{x}|<|\mathbf{x}'|$ and (B.3) tells that

$$\begin{aligned}
\int_{\mathbf{x}'\in\mathbb{D}\setminus\mathbb{D}_\varepsilon}H_0^{(2)}(\mathrm{k_b}|\mathbf{x}-\mathbf{x}'|)\mathrm{d}V' &= \int_{\mathbf{x}'\in\mathbb{D}\setminus\mathbb{D}_\varepsilon}\sum_{k=-\infty}^{\infty}J_k(\mathrm{k_b}\varepsilon)H_k^{(2)}(\mathrm{k_b}|\mathbf{x}'|)e^{\mathrm{i}k\phi}\mathrm{d}V' \\
&= \sum_{k=-\infty}^{\infty}J_k(\mathrm{k_b}\varepsilon)\int_0^{2\pi}e^{\mathrm{i}k\phi}\mathrm{d}\phi\int_\varepsilon^{\mathrm{a}}H_k^{(2)}(\mathrm{k_b}r)r\,\mathrm{d}r \\
&= J_0(\mathrm{k_b}\varepsilon)\frac{2\pi}{\mathrm{k_b}^2}\int_{\mathrm{k_b}\varepsilon}^{\mathrm{k_b a}}H_0^{(2)}(z)z\mathrm{d}z \\
&= J_0(\mathrm{k_b}\varepsilon)\frac{2\pi}{\mathrm{k_b}}\left(H_1^{(2)}(\mathrm{k_b a})\mathrm{a}-H_1^{(2)}(\mathrm{k_b}\varepsilon)\varepsilon\right).
\end{aligned} \tag{B.6}$$

For the first integral in (B.5) it holds that $|\mathbf{x}|>|\mathbf{x}'|$ and (B.3) tells that

$$\begin{aligned}
\int_{\mathbf{x}'\in\mathbb{D}_\varepsilon}H_0^{(2)}(\mathrm{k_b}|\mathbf{x}-\mathbf{x}'|)\mathrm{d}V' &= \int_{\mathbf{x}'\in\mathbb{D}_\varepsilon}\sum_{k=-\infty}^{\infty}J_k(\mathrm{k_b}|\mathbf{x}'|)H_k^{(2)}(\mathrm{k_b}|\mathbf{x}|)e^{\mathrm{i}k\phi}\mathrm{d}V' \\
&= \sum_{k=-\infty}^{\infty}H_k^{(2)}(\mathrm{k_b}\varepsilon)\int_0^{2\pi}e^{\mathrm{i}k\phi}\mathrm{d}\phi\int_0^{\varepsilon}J_k(\mathrm{k_b}r)r\,\mathrm{d}r \\
&= 2\pi H_0^{(2)}(\mathrm{k_b}\varepsilon)\int_0^{\varepsilon}J_0(\mathrm{k_b}r)r\,\mathrm{d}r \\
&= \frac{2\pi\varepsilon}{\mathrm{k_b}}H_0^{(2)}(\mathrm{k_b}\varepsilon)J_1(\mathrm{k_b}\varepsilon).
\end{aligned} \tag{B.7}$$

Substitution of (B.6) and (B.7) in (B.5) and taking the limit gives

$$\begin{aligned}
\hat{g}^{\mathrm{w}}(\mathbf{0},s) &= -\frac{\mathrm{i}}{4\pi \mathrm{a}^2}\lim_{\varepsilon\downarrow 0}\left[\frac{2\pi\varepsilon}{\mathrm{k_b}}H_0^{(2)}(\mathrm{k_b}\varepsilon)J_1(\mathrm{k_b}\varepsilon)+J_0(\mathrm{k_b}\varepsilon)\frac{2\pi}{\mathrm{k_b}}\left(H_1^{(2)}(\mathrm{k_b a})\mathrm{a}-H_1^{(2)}(\mathrm{k_b}\varepsilon)\varepsilon\right)\right] \\
&= -\frac{\mathrm{i}}{2\mathrm{k_b a}}\left(H_1^{(2)}(\mathrm{k_b a})-\frac{2\mathrm{i}}{\pi\mathrm{k_b a}}\right).
\end{aligned}$$

The weakened Green's function is therefore given by

$$\hat{g}^{\mathrm{w}}(\mathbf{x},s)=\begin{cases}-\frac{\mathrm{i}}{2\mathrm{ak_b}}H_0^{(2)}(\mathrm{k_b}|\mathbf{x}|)J_1(\mathrm{k_b a}) & \text{if } \mathbf{x}\notin\mathbb{D}\\ -\frac{\mathrm{i}}{2\mathrm{k_b a}}\left(H_1^{(2)}(\mathrm{k_b a})-\frac{2i}{\pi\mathrm{k_b a}}\right) & \text{if } \mathbf{x}=\mathbf{0}\end{cases}$$

and this function can be used to approximate the Green's function in all grid points.

BIBLIOGRAPHY

[1] W. M. Brink, A. M. van der Jagt, M. J. Versluis, B. M. Verbist, and A. G. Webb, *High permittivity dielectric pads improve high spatial resolution magnetic resonance imaging of the inner ear at 7 t,* Investigative radiology **49**, 271 (2014).

[2] N. Budko, *Electromagnetic radiation, scattering and imaging, delft 2004,* .

[3] M. van Beurden and S. van Eijndhoven, *Well-posedness of domain integral equations for a dielectric object in homogeneous background,* Journal of Engineering Mathematics **62**, 289 (2008).

[4] A. Polimeridis, J. Villena, L. Daniel, and J. White, *Stable fft-jvie solvers for fast analysis of highly inhomogeneous dielectric objects,* Journal of Computational Physics **269**, 280 (2014).

[5] P. Sonneveld and M. B. van Gijzen, *Idr (s): A family of simple and fast algorithms for solving large nonsymmetric systems of linear equations,* SIAM Journal on Scientific Computing **31**, 1035 (2008).

[6] J. Markkanen, C.-C. Lu, X. Cao, and P. Yla-Oijala, *Analysis of volume integral equation formulations for scattering by high-contrast penetrable objects,* Antennas and Propagation, IEEE Transactions on **60**, 2367 (2012).

[7] M. Van Beurden and S. van Eijndlioven, *Gaps in present discretization schemes for domain integral equations,* in *Electromagnetics in Advanced Applications, 2007. ICEAA 2007. International Conference on* (IEEE, 2007) pp. 673–675.

[8] P. Zwamborn and P. M. Van den Berg, *A weak form of the conjugate gradient fft method for two-dimensional te scattering problems,* Microwave Theory and Techniques, IEEE Transactions on **39**, 953 (1991).

[9] P. Zwamborn, P. M. Berg, *et al.*, *Computation of electromagnetic fields inside strongly inhomogeneous objects by the weak-conjugate-gradient fast-fourier-transform method,* JOSA A **11**, 1414 (1994).

[10] J. T. Fokkema and P. M. van den Berg, *Seismic applications of acoustic reciprocity* (Elsevier, 2013).

[11] C. A. Balanis, *Advanced engineering electromagnetics*, Vol. 20 (Wiley New York, 1989).